Hydrology and
Earth System
Sciences

Dominant controls of transpiration along a hillslope transect inferred from ecohydrological measurements and thermodynamic limits

Maik Renner[1], **Sibylle K. Hassler**[2,6], **Theresa Blume**[2], **Markus Weiler**[3], **Anke Hildebrandt**[4,1], **Marcus Guderle**[4,1,7], **Stanislaus J. Schymanski**[5], **and Axel Kleidon**[1]

[1]Max-Planck-Institut für Biogeochemie, Jena, Germany
[2]GFZ German Research Centre for Geosciences, Section Hydrology, Potsdam, Germany
[3]Universität Freiburg, Hydrologie, Freiburg, Germany
[4]Universität Jena, Ecological Modelling Group, Jena, Germany
[5]ETH Zürich, Department of Environmental Systems Science, Zurich, Switzerland
[6]Karlsruhe Institute of Technology, Institute of Water and River Basin Management, Karlsruhe, Germany
[7]Technische Universität München, Chair for Terrestrial Ecology, Department of Ecology and Ecosystemmanagement, Munich, Germany

Correspondence to: Maik Renner (mrenner@bgc-jena.mpg.de)

Abstract. We combine ecohydrological observations of sap flow and soil moisture with thermodynamically constrained estimates of atmospheric evaporative demand to infer the dominant controls of forest transpiration in complex terrain. We hypothesize that daily variations in transpiration are dominated by variations in atmospheric demand, while site-specific controls, including limiting soil moisture, act on longer timescales.

We test these hypotheses with data of a measurement setup consisting of five sites along a valley cross section in Luxembourg. Both hillslopes are covered by forest dominated by European beech (*Fagus sylvatica* L.). Two independent measurements are used to estimate stand transpiration: (i) sap flow and (ii) diurnal variations in soil moisture, which were used to estimate the daily root water uptake. Atmospheric evaporative demand is estimated through thermodynamically constrained evaporation, which only requires absorbed solar radiation and temperature as input data without any empirical parameters. Both transpiration estimates are strongly correlated to atmospheric demand at the daily timescale. We find that neither vapor pressure deficit nor wind speed add to the explained variance, supporting the idea that they are dependent variables on land–atmosphere exchange and the surface energy budget. Estimated stand transpiration was in a similar range at the north-facing and the south-facing hillslopes despite the different aspect and the largely different stand composition. We identified an inverse relationship between sap flux density and the site-average sapwood area per tree as estimated by the site forest inventories. This suggests that tree hydraulic adaptation can compensate for heterogeneous conditions. However, during dry summer periods differences in topographic factors and stand structure can cause spatially variable transpiration rates. We conclude that absorption of solar radiation at the surface forms a dominant control for turbulent heat and mass exchange and that vegetation across the hillslope adjusts to this constraint at the tree and stand level. These findings should help to improve the description of land-surface–atmosphere exchange at regional scales.

1 Introduction

Evapotranspiration E couples water and energy balances at the land surface and is constrained by both, the supply of water and the atmospheric demand for water. Total E is composed of evaporation from intercepted water on plants and the surface, soil evaporation, and the physiolog-

ical process of plant transpiration (E_T) taking water from the soil, groundwater, and possibly bedrock (Shuttleworth, 1993; Miller et al., 2010; Schwinning, 2010). Transpiration is of key importance for the (local) climate by altering the surface energy balance (Oke, 1987), and for water resources where E_T is an important loss term of the water balance (Federer, 1973; Jasechko et al., 2013). The tight coupling to photosynthesis and thus primary productivity makes E_T also central for agriculture and forestry. There is thus a need to understand the spatial and temporal variation of E_T as a result of interacting climatic and biogeophysical processes. Especially in temperate forests these biogeophysical feedbacks are poorly understood, which strongly reduces our ability to assess their role in mitigating climate change (Bonan, 2008).

Forests are often found in complex topographical settings. Thus, we have to consider that the first-order physical controls on E are strongly altered by topography: hillslope angle and aspect systematically alter the amount of absorbed solar radiation and thus atmospheric demand (Baumgartner, 1960; Lee and Baumgartner, 1966; Ivanov et al., 2008), whereas slope and the topographic setting, such as contributing area, alter the lateral redistribution of water (Famiglietti et al., 1998; Bachmair and Weiler, 2011). Apparently, forests adjust to these conditions, but little is known how vegetation and site-scale transpiration in particular respond to these topographically altered boundary conditions of water supply and demand (Tromp-van Meerveld and McDonnell, 2006). For example Holst et al. (2010) found that detailed forest hydrological models yielded different trends of simulated mean stand transpiration when comparing European beech stands on different hillslope aspects. These differences add up when simulating runoff generation from these sites and emphasizes the difficulty in the assessment of forest water balance in complex terrain.

Although detailed models of various feedbacks between plant physiology and the environmental conditions are available (Monteith, 1965; Farquhar et al., 1980; Wang and Jarvis, 1990; Whitehead, 1998; Haas et al., 2013) their applicability is generally restricted by the need for detailed physiologic, atmospheric, and soil parameters. As an alternative to improve our understanding by increasingly detailed modeling, several authors proposed to deduce and predict E through physical and physiological constraints (Calder, 1998; West et al., 1999; Raupach, 2001; Zhang et al., 2008; Wang and Bras, 2011). Applications of these fundamental constraints do not only increase our understanding of the soil–plant atmosphere continuum, they may also lead to a few but independent predictors of E. For example, Kleidon and Renner (2013b) applied thermodynamic limits of convective heat exchange to the surface–atmosphere system. They found that under the assumption of maximum convective power and no surface water limitation, atmospheric demand is only dependent on absorbed solar radiation and surface temperature, being consistent with the empirical formulations of potential evaporation of Makkink (1957) and the well-known equilib-

rium evaporation concept (Schmidt, 1915; Priestley and Taylor, 1972; de Bruin et al., 2016). Contrary to the classic formulation of Dalton (see Brutsaert (1982) for an overview), where vapor pressure deficit (VPD) and wind speed are used as forcing variables of potential evapotranspiration, Kleidon and Renner (2013b) argued that VPD and wind speed emerge from the land–atmosphere interaction. The practical implication of maximum convective power is that atmospheric demand can be estimated without these variables and empirical parameters.

In this study we aim to assess the dominant temporal and spatial controls of forest transpiration in complex terrain. Therefore, we use the parsimonious approach of maximum convective power to estimate potential evaporation. The approach of maximum convective power has so far only been applied for long-term annual estimates of E and large-scale geographic variations (Kleidon et al., 2014). Here we test this approach at the site level and for daily timescales in complex topographical terrain. We use data of a well-instrumented beech forest with measurement sites across a transect with a north-facing and a south-facing hillslope. The indirect assessment of E_T is based on ecohydrological measurements of sap flow and soil moisture. We present a systematic analysis to address the question of how much transpiration varies in complex terrain and what measurable site characteristics influence forest transpiration. In particular we hypothesize that potential evaporation representing the atmospheric demand for water can be estimated by thermodynamic limits of convection, which only relies on surface absorption of solar radiation and temperature. Specifically, we test how much of the daily variations of in situ transpiration observations can be explained by atmospheric demand and by how much they respond to atmospheric demand along the measurement transect. Therefore, we perform a linear regression and correlation analysis of the transpiration estimates to atmospheric demand comprising daily data of the growing season. Further, we evaluate how much additional variance can be explained by other time-varying parameters such as VPD, wind speed, and soil moisture. Differences in the strength of correlation between sites would imply that site-dependent, time-varying constraints on transpiration are relevant. In contrast, a high, consistent correlation would imply that atmospheric demand and thus energy limitation of transpiration is the dominant driver of day to day variability. The overall response of transpiration to atmospheric demand represented by the slope of the linear regression would then indicate the importance of site-dependent controls such as topographic, soil, and plant factors.

2 Methods

2.1 Site description

We analyze measurements at six different sites along a well-instrumented steep forested hillslope transect (north-facing vs. south-facing; see Fig. 1) in the Attert catchment in Luxembourg over the vegetation period of 2013. The hillslope transect is part of the Catchments As Organized Systems (CAOS) field observatory (Zehe et al., 2014) and is located in the western part of Luxembourg ($5°$ E $48'13''$, $49°$ N $49'34''$) at about 460 m NN. The land cover of the transect is a mixed forest dominated by European beech (*Fagus sylvatica* L.). The north-facing slope has an inclination of $\approx 15°$ and is composed of a few dominant trees with large gaps and dense understorey mainly of young beech trees, whereas the south-facing slope is generally steeper ($\approx 22°$) and has no understorey and a denser canopy. Also tree species composition varies between slopes, with 97 % beech on the north-facing sites with single spruce trees and 90 % beech and 10 % oak on the south-facing sites. The valley site has 80 % beech with 10 % spruce and alder. Geologically, the site is situated in northeast–southwest-trending fold system of Schists of the Ardennes Massif. The shallow soils developed on periglacial slope deposits (Juilleret et al., 2011). The deposits are generally found at a depth of 70–90 cm.

Standard meteorological data, global radiation, air temperature, relative humidity, and wind speed were measured 2 m above ground at all sites. For the meteorological forcing we used the data from the open grassland site G1, which is located 240 m to the northwest of the forest site N1; see Fig. 1. Absorbed solar radiation $R_{sn} = (1 - \alpha) R_g$ in W m^{-2} is derived from global radiation R_g and an albedo estimate of $\alpha = 0.15$, which is representative for deciduous forests (Oke, 1987).

2.2 Estimation of atmospheric demand

Our aim is to estimate the potential evaporation from first principles and with few, independent input data. Therefore we make use of the concept of thermodynamic limits of convection, which was recently established by Kleidon and Renner (2013b) and used successfully to estimate the sensitivity of the hydrologic cycle to global warming (Kleidon and Renner, 2013a; Kleidon et al., 2015) and for grid-based global-scale predictions of annual average terrestrial evaporation (Kleidon et al., 2014). Here we only illustrate how the concept is used to estimate potential evaporation; for further details the reader is referred to the mentioned publications.

Convection can be thought of as a heat engine, which converts a temperature gradient into kinetic energy (Ozawa et al., 2003). To capture the fundamental trade-off of thermodynamic limits of convective exchange, we consider a simple two-box surface–atmosphere system in steady state, which is sketched in Fig. 2. We consider the steady-state energy

balance of the surface $R_{sn} = J + R_{ln}$. The surface is heated by absorption of incoming solar radiation R_{sn}. The turbulent heat fluxes J and the net longwave exchange R_{ln} both cool the surface. The turbulent heat fluxes are composed of the sensible (H) and latent heat flux (λE). Longwave radiative exchange is represented by a simplified linearized radiation $R_{ln} = k_r(T_s - T_a)$, with T_s being the temperature of the surface and T_a the temperature of the atmosphere and k_r being a constant radiative exchange coefficient. The power of the convective heat engine G is fundamentally limited by the Carnot limit:

$$G = J \frac{T_s - T_a}{T_s}. \tag{1}$$

Different from the classic Carnot engines, the convective heat engine has flexible boundary conditions, namely, the temperature gradient $T_s - T_a$ responds to the strength of the convective heat fluxes J through its coupling to the surface energy balance. Rearranging the surface energy balance

$$T_s - T_a = \frac{R_{sn} - J}{k_r} \tag{2}$$

shows that a stronger convective heat flux at a given radiation reduces the temperature gradient. This effectively yields a thermodynamic limit of the maximal power of the convective heat engine. The limit is obtained by inserting this feedback into the Carnot limit Eq. (1) and solving for the maximum with respect to J. Hypothesizing that convection actually operates at this limit (subscript opt), we obtain a closure for the strength of convective fluxes:

$$J_{opt} = \frac{R_{sn}}{2}. \tag{3}$$

Once the convective fluxes are obtained we aim to estimate the partitioning into sensible and latent heat fluxes. Using the Bowen ratio B and bulk formulations for sensible (H) and latent heat fluxes (λE), we can write

$$B = \frac{H}{\lambda E} = \frac{\rho c_p k_h}{\rho \lambda k_e} \frac{T_s - T_a}{q_s - q_a} = \frac{c_p}{\lambda} \frac{T_s - T_a}{q_s - q_a} \tag{4}$$

where $c_p = 1.2$ J K^{-1} kg^{-1} is the heat capacity of air, $\rho = 1$ kg m^{-3} the air density, $\lambda = 2.5 \times 10^6$ J kg^{-1} the latent heat of vaporization, q_s and q_a being the specific humidity (g kg^{-1}) at the surface and the atmosphere, respectively. If we assume that the air at the surface and in the atmosphere is saturated with water vapor and that the slope of the saturation vapor pressure curve ($s = \partial e_{sat} / \partial T$) is invariant within this range, the vertical humidity gradient can be written as $q_s - q_a = s(T_s - T_a) \cdot 0.622 / p_s$. e_{sat} is the temperature-dependent vapor pressure at saturation, p_s the surface pressure (hPa) and 0.622 being the ratio of the gas constants for air and water vapor. Introducing the psychrometric constant with $\gamma = c_p / \lambda \cdot p_s / 0.622 \approx 65$ Pa K^{-1} and assuming that the
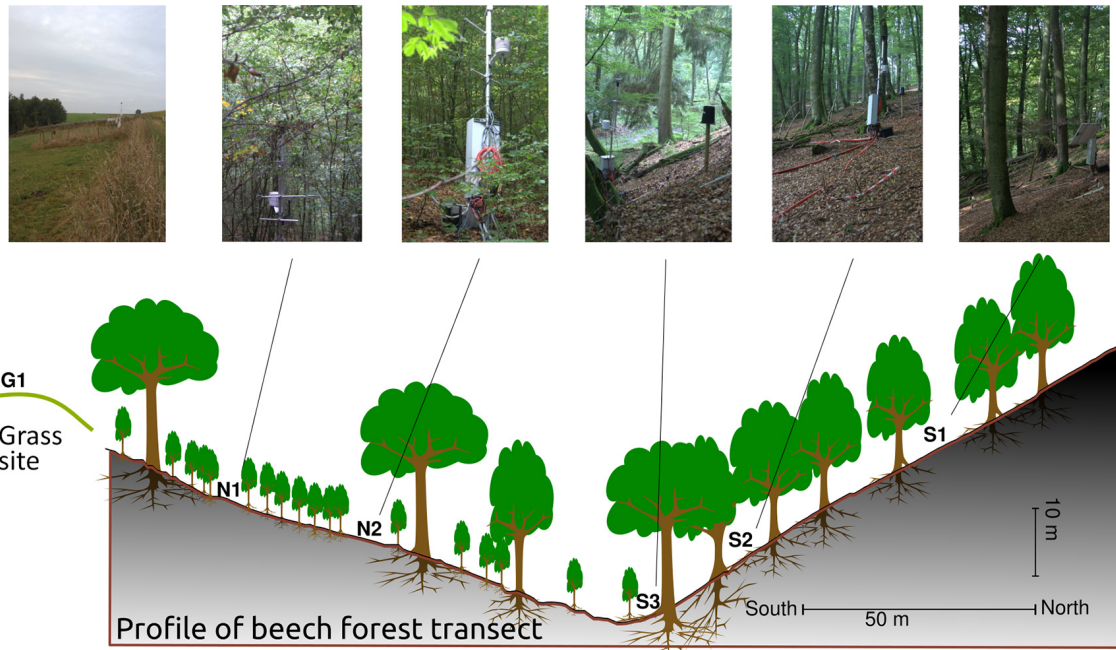
Figure 1. Measurement setup along a hillslope transect. Captital letters indicate aspect of the sites (N: north-facing, S: south-facing) and the numbering represents the position of the site on the hillslope: upslope (1), midslope (2), and downslope (3).
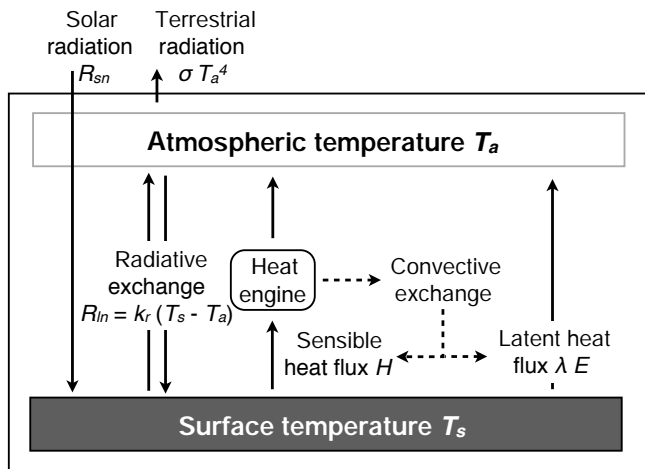

Figure 2. Land–atmosphere energy balance scheme for derivation of atmospheric demand adapted after Kleidon et al. (2014).

vertical exchange coefficients of air k_h and of vapor k_e are equal, we thus obtain the equilibrium Bowen ratio $B = \frac{\gamma}{s}$ (Schmidt, 1915; Stull, 1988). The equilibrium Bowen ratio depends only on temperature, because s is a nonlinear function of temperature and γ is approximately constant. We determine s by an empirical equation (Bohren and Albrecht, 1998): $s = s(T) = 6.11 \cdot 5417 \cdot T^{-2} \cdot e^{19.83 - 5417/T}$ with temperature T (K).

Combining the equilibrium Bowen ratio with the concept of maximum convective power we obtain an expression for the potential evaporation, herein referred to as atmospheric demand E_{opt} (Kleidon and Renner, 2013b; Kleidon et al., 2014):

$$E_{opt} = \frac{1}{\lambda} \frac{s}{s+\gamma} \frac{R_{sn}}{2}. \tag{5}$$

Hence, only absorbed solar radiation R_{sn} and temperature data are required to estimate atmospheric evaporative demand, when derived from thermodynamic limits using simplifying assumptions on longwave radiative exchange and the assumption for the equilibrium Bowen ratio.

We also compare our results with the well-established FAO Penman–Monteith grass reference evaporation equation (Allen et al., 1998):

$$E_{PM} = \frac{0.408 \, s (R_n - G) + \gamma \frac{900}{T+273} u \text{VPD}}{s + \gamma (1 + 0.34 \, u)}, \tag{6}$$

where R_n is net radiation, G the ground heat flux, T air temperature, u wind speed (both in 2 m height), and VPD is the saturation vapor pressure deficit in kilopascal (kPa). Equation (6) is a modified Penman–Monteith equation for a standardized grass surface at a daily resolution. As input variables we use the same variables as for E_{opt} (daily average air temperature, shortwave radiation) and in addition net radiation, ground heat flux, relative humidity, and wind speed. Because net radiation was not measured at our sites we used an empirical formulation for R_n (Allen et al., 1998, Eq. (39)). Therefore, data of daily minimum and maximum temperature as well as information on the day of year and

latitude were required. The soil heat flux was estimated as $G = 0.1 \cdot R_n$.

2.3 Topographic effects on shortwave radiation

In complex terrain the incoming radiation is influenced by the slope and the aspect of the current position (Kondratyev and Fedorova, 1977). To account for these effects we use a topographic radiation correction method, which projects the extraterrestrial irradiance on inclined surfaces implemented in the software *r.sun* (Šúri and Hofierka, 2004), which is part of the open-source Geographic Information System (GIS) platform GRASS GIS (http://grass.osgeo.org). *r.sun* estimates potential clear-sky spatial global radiation $R_{g,pot}$ fields for each day of year. To account for cloudy conditions we use the open-field site G1 as a reference station and estimate a daily cloud factor $f_c = R_{g,G1} / R_{g,pot}$ using the closest grid point of the respective site. Then $R_{g,pot}$ is multiplied with f_c to obtain a radiation estimate for the sites in the forest $R_{g,c}$. As input for *r.sun* we use a 10 m resolution Digital Elevation Model (DEM) (with slope and aspect inputs from the DEM) and default parameters (Linke atmospheric turbidity coefficient $= 2$). We thus estimate global radiation on a tilted surface (aspect, slope) and also include topographic shading effects. The effect is largest when the sun angle is low (autumn–winter–spring) and decreases R_g and thus E_{opt} at the north-facing slope while increasing it on the south-facing slope; see Fig. S1 in the Supplement. These estimates are generally consistent with radiative observations in sloped terrain (Holst et al., 2005).

2.4 Biometric measurements

A forest inventory for all sites was done in March 2012. The circumference at breast height of all trees with circumference larger or equal to 4 cm was measured in a 20 m by 20 m plot for each site. Stem basal area was calculated and a total stand basal area was computed for each site.

Leaf area index (LAI) was measured with a LICOR LAI-2200 plant canopy analyzer at all forested sites in two campaigns. The summer campaign was carried out on 11 August 2012 and the winter campaign on 20 March 2014. Here we use the measurements taken with all rings of the LAI-2200. The LAI was averaged from 36 measurements points per site. The difference between summer and winter LAI should reveal the actual leaf area index without stems and topographic shading effects.

2.5 Sap flow measurements and upscaling stand transpiration

The five forested sites are instrumented with multiple sap flow sensors (four trees at each site, installed between mid-May to November). Heat pulse sensors (East 30 Sensors, Pullman, Washington 99163 USA) based on the heat ratio method (Burgess et al., 2001) have been used as they are

less susceptible to natural heating gradients, and require less electrical power (Vandegehuchte and Steppe, 2013). The sensors measure the heat pulse velocity, which is corrected for wounding and sensor alignment; see Sect. A1 in the appendix. The heat pulse velocity is then converted into sap flux density, SFD ($cm^3 cm^{-2} h^{-1}$) (Burgess et al., 2001):

$$SFD = v_c \frac{\rho_b (c_w + m_c c_s)}{\rho_s c_s}. \tag{7}$$

Thus, to estimate the sap flux density, knowledge of xylem wood properties, namely, the basic density of wood ρ_b, the density of the sap ρ_s, the specific heat capacity of the wood matrix c_w, and of the sap c_s as well as the water content of the xylem is required. For sap we use the standard parameters for water at 20° C, with $\rho_s = 1 \, kg \, cm^3$, $c_s = 4182 \, J \, kg^{-1} \, K^{-1}$. The heat capacity of the woody matrix is generally given with $c_w = 1200 \, J \, kg^{-1} \, K^{-1}$ (Burgess et al., 2001). The basic density of sapwood ρ_b measured as dry weight over green volume and the moisture content of the xylem m_c are species-specific parameters. We used $\rho_b = 0.61 \, kg \, cm^{-3}$ and $m_c = 0.7$ for the xylem of European beech estimated by Glavac et al. (1990). They sampled about 260 trees at two different sites between 35 and 42 years old over the course of 1 year. For the thermal diffusivity of the xylem, we used a fixed value of $k_w = 2.5 \times 10^{-3} \, cm^2 \, s^{-1}$ (Burgess et al., 2001).

The raw measurements obtained every 30 min were quality controlled and suspect data were filtered before further analysis was performed. At three larger trees the outermost sensor readings were replaced by the second sensor depth reading because their annual mean was smaller than the inner sensors, which indicates a sensor misplacement into the bark of the tree. The sensors measure the heat pulse velocities at three different radial depths in the tree. The daily mean sap flux density per tree is obtained by an average of all readings per depth and day. Units of SFD were converted to $m^3 m^{-2} d^{-1}$. An arithmetic mean of the tree-average sap flux density was used to obtain the site-average sap flux density.

Measurements of sap flux density only provide a relative measure of the velocity of the ascending xylem sap. To obtain tree water fluxes a representative xylem area per sensor depth is assumed, which is then multiplied with the corresponding sap flux density (Burgess et al., 2001). Tall trees with a diffuse-porous xylem structure such as beech are known to have a large sapwood to basal area ratio (Köstner et al., 1998). Further, the radial profile of the sap flux density varies in these trees. Therefore, deep measurements are ideally required (Gebauer et al., 2008). In the absence of these deeper measurements, we follow the reasoning of Lüttschwager and Remus (2007) to derive uncertainty ranges for the inner conducting sapwood area; see appendix.

To upscale to the site level we use the inventory data, which provides the number of trees in the stand, diameter at breast height (DBH), and species information. Daily sap flux density per sensor depth was averaged for each species and tree status (dominant vs. suppressed) for each site. Miss-

ing sap flux density data were filled by linear regression with neighboring sites. The largest data gaps were filled at sites N2 and S2. Finally, the upscaled daily stand transpiration was obtained by summing up the product of sap flux density per depth D and sap wood area per depth $A_s(D)$ for all trees and dividing by the area of the inventory A_{stand}:

$$E_{sap} = \frac{1}{A_{stand}} \sum_{tree=1}^{n} \sum_{D=1}^{3} (SFD(D)A_s(D)). \quad (8)$$

2.6 Root water uptake estimation

As another means to estimate transpiration we use soil moisture measurements. Soil moisture sensors (Decagon 5TE soil moisture sensors, with an accuracy of $\pm 3\%$ volumetric water content and resolution of 0.08%) are installed at three profiles at each site at 10–30–50 cm depth and one deeper sensor (approx. 70 cm) at one of the profiles. There is a range of methods to estimate root water uptake from soil moisture observations (Shuttleworth, 1993; Cuenca et al., 1997; Wilson et al., 2001; Schwärzel et al., 2009; Breña Naranjo et al., 2011; Guderle and Hildebrandt, 2015). Here, we employ a simplified soil water budget method to estimate daily root water uptake E_{RWU} (units mm d^{-1}). The method is based the daytime reduction of measured soil moisture integrated over the soil profile. To avoid the influence of infiltration and other fluxes, which are not caused by root water uptake E_{RWU}, we filtered the days with significant nighttime soil moisture variations as well as rainy days. A representative site value of E_{RWU} was derived by averaging the estimates of all three soil profiles. Details of the method can be found in the Appendix A3.

2.7 Statistical analyses

To test if the transpiration estimates are driven by potential atmospheric demand, we use linear ordinary least squares (OLS) regression with the transpiration estimates as response variable and E_{opt} as independent variable. The slope of the regression with sap flux density is denoted by $b_{SFD} = \frac{dv_{sap}}{dE_{opt}}$ with units $[m^3 m^{-2} d^{-1}] / [mm d^{-1}]$. For E_{sap} the slope is denoted $b_{sap} = \frac{dE_{sap}}{dE_{opt}}$ and for E_{RWU} the slope is denoted $b_{RWU} = \frac{dE_{RWU}}{dE_{opt}}$. The latter two regression slopes have non-dimensional units $[mm d^{-1}] / [mm d^{-1}]$. To estimate the potential influence of other independent variables on transpiration, such as soil moisture or vapor pressure deficit, we use the residuals of the OLS regression as response variable of a further linear regression. The explanatory power of the other variable is reported by the adjusted explained variance (denoted by R_θ^2 for soil moisture effects), which is a diagnostic of the OLS regression.

Note that by using time series of daily data, which are shaped by the seasonal cycle, the assumption of independence of the predictor variables in the linear regression is
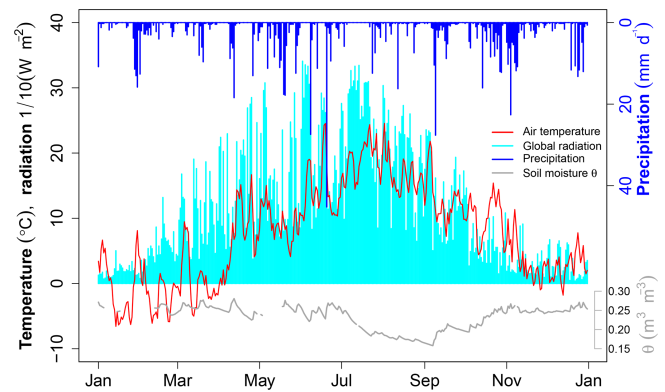

Figure 3. Meteorological forcing and average soil moisture at the grassland site (G1) for 2013. A few data gaps were filled with data from nearby grassland sites.

not often justified. The effect of serial dependence generally does not bias the regression coefficients, but reduces the statistical significance of a regression. Therefore, we estimate the standard deviation of the regression coefficient (σ_{slope}) and its reported significance with a pre-whitening procedure of Newey and West (1994) provided by function *coeftest* of the R packages lmtest (Zeileis and Hothorn, 2002) and sandwich (Zeileis, 2004). All data analysis was done in R (R Core Team, 2016) and the R-package data.table (Dowle et al., 2014).

3 Results

3.1 Meteorological observations in 2013

Daily time series of temperature, global radiation, precipitation, and site-average soil moisture content for 2013 are shown in Fig. 3. The average annual (growing season, May–October) temperature was 7.9 (13.7) °C, with an average global radiation of 117 (169) W m^{-2}. The highest temperatures were observed in a short period in June and a longer period between mid-July and August. We observed a total annual precipitation of 866 mm (no catch correction applied), which was, however, unevenly distributed throughout the year. Most precipitation fell in June (110 mm), with low rainfall during July and August (34 and 38 mm, respectively) and more rainfall in the autumn months. Hence, the soil moisture recession lasted from July to September (bottom gray line in Fig. 3).

3.2 Site-scale transpiration estimates

Two independent site-scale transpiration estimates are evaluated in the following. The first estimate, E_{sap}, was obtained by upscaling sap flow measurements with the forest plot inventory data. The second estimate was derived by averaging E_{RWU} of the 2–3 soil profiles per site. Both transpiration

Table 1. Seasonal totals in mm of estimated stand transpiration E_{sap} and potential evaporation E_{opt} and E_{PM}. For the totals we used the period 12 May 2013–31 October 2013. For E_{sap} we present a range of estimates with minimal, linear decline and maximal estimate with respect to the depth of conducting inner sapwood (Eqn. A3, A4, and A5).

Site	E_{sap} min–lin–max	E_{opt}	E_{PM}
N1	106–128–156	240	351
N2	76–115–164	232	345
S3	127–176–244	296	387
S2	104–129–170	293	386
S1	96–122–160	295	387
G1		270	371

estimates are shown as daily time series for site N1 at the north-facing and S1 at the south-facing hillslope in Fig. 4. The north-facing sites have lower potential evaporative demand (estimated by topographically corrected incoming solar radiation) than the south-facing sites. Variations of daily soil water contents are quite similar between the sites. However, the north-facing site is on average slightly wetter ($\overline{\theta} = 0.21 \pm 0.04$) than the south-facing site ($\overline{\theta} = 0.18 \pm 0.03$). There is a large temporal variability in the atmospheric forcing represented by E_{opt}, which is also found for both transpiration estimates. The highest transpiration rates are seen in the dry and sunny period in July. Comparing the sites at the different hillslopes we find similar magnitudes of E_{sap}. However, E_{RWU} is found to be much higher than E_{sap} in spring and early summer at the north-facing sites.

Seasonal totals of E_{sap} and potential evaporation are reported in Table 1. The E_{sap} estimates for the upper north and south-facing hillslope sites are relatively similar. The highest E_{sap} is estimated at the valley bottom site S3, which amounts to a difference of about 50 mm for the seasonal total. Large uncertainty in the nominal value of E_{sap} is due to the assumed depth of the sapwood, which is estimated from data of the innermost sensor and allometric relationships of sapwood. Thereby the range between different conducting sapwood depths is largest at the valley site because there are more tall trees where this uncertainty matters.

3.3 Transpiration response to atmospheric demand

To test if the transpiration estimates are driven by potential atmospheric demand, we performed a linear regression of the site-average values with E_{opt} as independent variable. We found that E_{sap} was relatively low in May and early June after leaf out and after mid-October with leaf senescence. In order to avoid phenological effects in the statistical analysis, we restrict the following analyses to the vegetation period from 10 June to 20 October. Respective scatter plots are shown in Fig. 5 and a summary of the results is reported in Table 2.
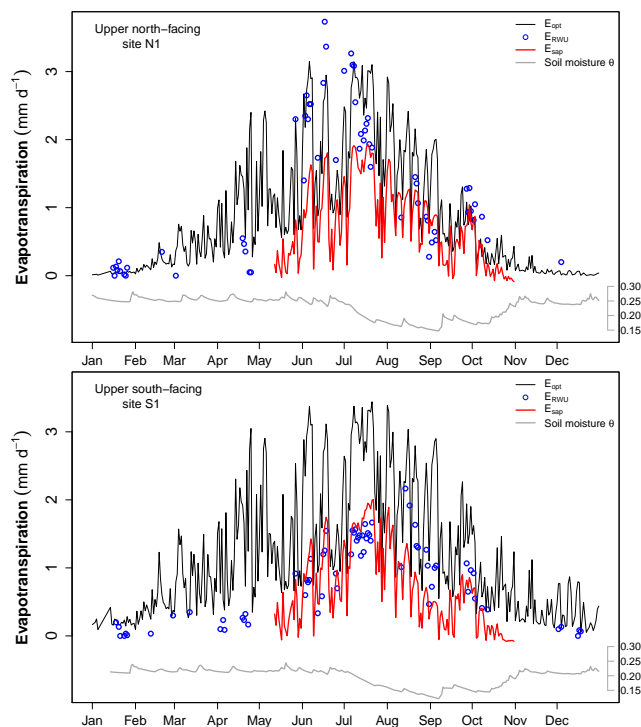

Figure 4. Time series of evapotranspiration estimates for north-facing hillslope site N1 in the left panel and south-facing site S1 in the right panel. E_{opt} is the potential evaporation derived from maximum power, E_{RWU} (blue points) and E_{sap} are transpiration estimates.

Figure 5 shows that both observations almost linearly increase with E_{opt}. For E_{sap} we find very high linear correlations with an average of $r^2_{E_{opt}} = 0.82$ (Table 2). The relatively large temporal variability in E_{sap} seen in Fig. 4 with a coefficient of variation CV = 0.68 across all forest sites is explained by the atmospheric demand E_{opt} (CV = 0.53). It is interesting to note that across all forest sites global radiation has only a slightly lower average $r^2 = 0.79$, whereas air temperature with $r^2 = 0.55$ and vapor pressure deficit with $r^2 = 0.66$ have less explanatory power. The correlation of site-average E_{RWU} to E_{opt} is much lower ($r^2 = 0.49$, averaged among all sites) than the correlation of E_{sap} to E_{opt}. All meteorological variables show lower correlations to E_{RWU} than to E_{sap}, which indicates a larger uncertainty of the soil moisture-derived transpiration estimate.

We also tested if the regression residuals show correlations with other daily observations. The reported adjusted squared correlation of a linear regression of the residual with VPD, wind speed, and soil moisture at the site level is reported in Table 2. Vapor pressure deficit does not explain residual variance of E_{sap} or E_{RWU}. Also wind speed does not show residual correlation for E_{sap} but higher positive residual correlation is found for E_{RWU} at the lower sites N2, S2, and significant at S3. Both of these variables are used as external

Table 2. Regression statistics for E_{sap} and E_{RWU} to E_{opt}, with n providing the number of observations (days). The slope and intercept are reported with the estimated standard deviation of the coefficients with $\pm\sigma$. Significance of the coefficients is indicated by stars: $p < .001$, ***; $p < .01$, **; $p < .05$, *. $r^2_{E_{opt}}$ and $r^2_{E_{PM}}$ are the linear squared correlation coefficients to E_{opt} and E_{PM}, respectively. The last three columns report the adjusted explained variance of a linear regression of the regression residuals for daily average vapor pressure deficit (R^2_{VPD}), daily average wind speed (R^2_u), and daily site-average volumetric water content (R^2_θ).

Variable	Site	n	Slope	Intercept	$r^2_{E_{opt}}$	$r^2_{E_{PM}}$	R^2_{VPD}	R^2_u	R^2_θ
E_{sap}	N1	130	0.61 ± 0.02***	-0.03 ± 0.05	0.88	0.89	0.01	0.00	0.02
	N2	129	0.57 ± 0.03***	-0.03 ± 0.05	0.88	0.89	0.01	0.01	-0.00
	S3	130	0.84 ± 0.08***	-0.36 ± 0.10***	0.83	0.87	-0.01	0.01	0.19**
	S2	109	0.62 ± 0.07***	-0.27 ± 0.09**	0.75	0.80	-0.01	0.01	0.25*
	S1	130	0.58 ± 0.07***	-0.23 ± 0.07**	0.78	0.83	-0.01	0.00	0.24**
E_{RWU}	N1	36	0.77 ± 0.18***	0.19 ± 0.27	0.52	0.50	0.04	0.03	0.64***
	N2	30	0.76 ± 0.19***	0.20 ± 0.40	0.67	0.69	-0.02	0.10	0.11
	S3	35	0.56 ± 0.11***	-0.21 ± 0.22	0.44	0.55	-0.03	0.32**	0.53***
	S2	30	0.52 ± 0.11***	0.11 ± 0.19	0.47	0.58	-0.02	0.12	0.45
	S1	39	0.44 ± 0.03***	0.13 ± 0.06*	0.63	0.60	-0.03	0.03	-0.02
	G1	28	0.75 ± 0.34*	0.32 ± 0.77	0.22	0.21	0.04	-0.04	0.63***

forcing in the Penman equation. Therefore, we calculated the squared correlation also for the FAO Penman–Monteith reference evaporation E_{PM}, Eq. (6). One can see from Table 2 that $r^2_{E_{PM}}$ is fairly similar, follows the same pattern, and is on average only slightly larger ($r^2_{E_{PM}} = 0.86$) than the correlation of E_{sap} to E_{opt}. Note that E_{PM} is on average 1.44 times larger than E_{opt} with a correlation between E_{PM} and E_{opt} of $r^2 = 0.98$.

In contrast to the meteorological variables, we found that the residuals are significantly correlated to the site-average soil moisture content at some sites. E_{sap} is significantly affected by soil moisture deficits at the south-facing sites. At these sites we find significant residual correlation of soil moisture $0.19 < R^2_\theta < 0.25$, which results in lower correlation to E_{opt} as compared to the two north-facing sites. Further, we find significant negative intercepts in the $E_{sap}-E_{opt}$ relationship. Even more affected by soil water limitation is E_{RWU} with significant values of $R^2_\theta > 0.5$ at N1, S3, and G1. However, at S1 there is no residual correlation at the site average level, but this is probably an effect of deriving a representative site-average from E_{RWU} profile estimates, because one soil profile at S1 actually shows a significant residual correlation (Table S3 in the Supplement). The potential effect of soil moisture on transpiration is visualized by the size of the symbols in Fig. 5. Thereby, E_{RWU} tends to be above the regression line under moist and warm conditions in early summer particularly at sites N1 and G1.

Figure 5 and the regression statistics allow for a further comparison of E_{sap} and E_{RWU}. Generally there is a good agreement of both estimates with $0.5 < r^2 < 0.9$, but there are site-specific deviations between the site transpiration estimates. The upper south-facing sites S1 and S2 agree well in magnitude, while E_{sap} for site S3 appears to have an offset of about $0.5\,\mathrm{mm\,d^{-1}}$. This offset could be influenced by the

apparent site heterogeneity. The site is situated in the transition between the steep hillslope and the riparian zone of the nearby creek. The E_{sap} upscaling represents this transition zone by the 20 m by 20 m forest inventory size and assumes constant sapwood properties for all trees within this site. On the other hand, three soil moisture profiles may be too few in this heterogeneous zone, which complicates the estimation of a representative site-average E_{RWU} value. At the north-facing sites we find that E_{sap} is lower than the E_{RWU} estimates. Especially during early summer when soil moisture was still high, E_{RWU} was found to be almost twice as large as E_{sap} and of similar magnitude as E_{opt} at these sites. However, there was a better agreement in late summer, when soil moisture declined; see Fig. 4. This indicates that the root water uptake estimates tend to be higher under moist conditions, which is reflected by the positive residual correlation to soil moisture reported in Tables 2 and S3 in the Supplement.

3.3.1 Response at tree level

By using tree-averaged sap flow density measurements directly we can assess how strong single trees respond to E_{opt}. Results of a linear regression analysis of daily tree average SFD to E_{opt} are reported in Table 3 (see also Fig. S3 in the Supplement). SFD of every tree shows a strong linear relation to E_{opt}, with varying slopes and intercept terms. Because most of the variability is explained by E_{opt}, we can simply compare the slope of the regression b_{SFD}. First, we find that b_{SFD} is especially high at the tall beech trees at the north-facing sites (1.26–$1.64\,\mathrm{[m^3\,m^{-2}\,d^{-1}]/[mm\,d^{-1}]}$), Table 3). These sampled tall trees at the north-facing sites are dominant trees without other tall trees in their vicinity. All other trees show much smaller values of b_{SFD} (0.26–$0.88\,\mathrm{[m^3\,m^{-2}\,d^{-1}]/[mm\,d^{-1}]}$). Second, we find that b_{SFD} is on
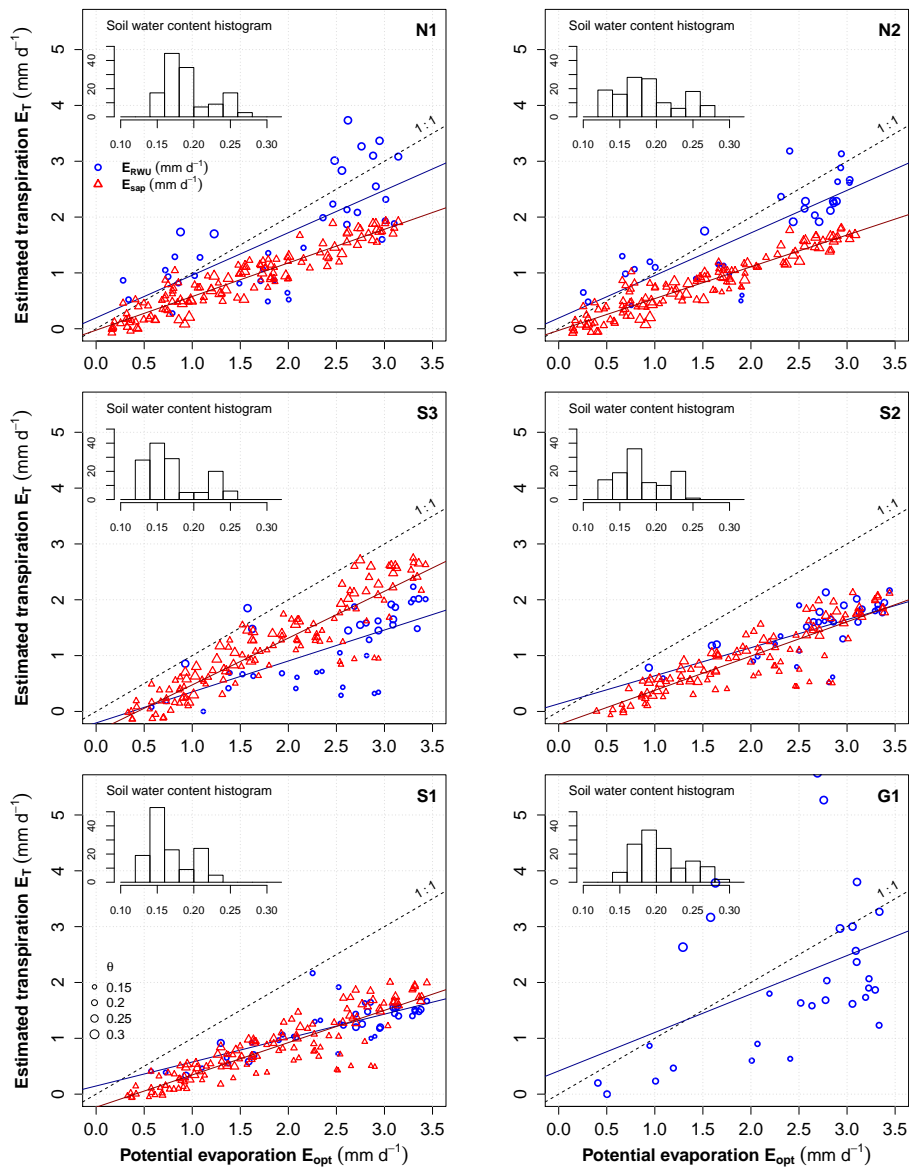
Figure 5. Site-average E_{RWU} (blue circles) and E_{sap} (red triangles) as function of E_{opt} during vegetation period (10 June–20 October) in 2013. Each panel presents data of one site (see Fig. 1 for site identifiers). The size of the symbols corresponds to the daily average soil moisture content. The histogram shows the distribution of site-average soil moisture. Solid lines depict the linear regression as tabulated in Table 2.

average larger at the north-facing than at the south-facing trees. Last, we also find that the oak tree at site S1 has the lowest b_{SFD}. For these reasons the upscaling of SFD to E_{sap} was done for each site separately and distinction was made between dominant and small trees as well as between species.

The residual regression analysis shows a similar pattern as the site-average values, with low influence of wind speed and VPD. Site-average soil moisture content (θ) shows significant effects at 9 out of 14 trees; see Table 3. Thereby all beech trees at the south-facing sites show an influence of θ on the sap flow residuals, with a maximum adjusted explained variance of $R_\theta^2 = 0.4$ at the upper south-facing site S1. In ad-

dition, the 3 of 4 small beech trees at the north-facing sites show significant influences of θ.

3.3.2 Soil profile response and root water uptake profiles

Generally, the measurement setup allows one to differentiate between three different levels of aggregation of root water uptake estimates: site-average, per profile, and per depth of the sensor.

Root water uptake per profile is obtained by summing up the estimates of each sensor. We find that 15 out of 16 pro-

Table 3. Regression statistics of daily SFD as average per tree and per site as extra row. Column DBH is the diameter at breast height in centimeters. n is the number of observations (days). The slope b_{SFD} and intercept of the linear univariate regression of SFD to E_{opt} with $\pm\sigma$ reporting the estimated standard deviation of the coefficients. Significance of the coefficients is indicated by stars: $p < .001$, ***; $p < .01$, **; $p < .05$, *. $r^2_{E_{\mathrm{opt}}}$ and $r^2_{E_{\mathrm{PM}}}$ are the linear squared correlation coefficients of SFD to E_{opt} and E_{PM}, respectively. The last three columns report the adjusted explained variance of a linear regression of the regression model residuals for the variables: vapor pressure deficit (R^2_{VPD}), wind speed (R^2_u), and site-average volumetric water content (R^2_θ).

Site	Tree	Species	DBH	n	b_{SFD}	Intercept	$r^2_{E_{\mathrm{opt}}}$	$r^2_{E_{\mathrm{PM}}}$	R^2_{VPD}	R^2_u	R^2_θ
N1	1	beech	66	130	1.30 ± 0.05***	0.09 ± 0.13	0.88	0.88	0.03	0.07**	0.11**
N1	2	beech	58	130	1.26 ± 0.04***	-0.06 ± 0.08	0.92	0.84	0.00	0.03*	-0.01
N1	3	beech	9	130	0.88 ± 0.05***	-0.08 ± 0.09	0.82	0.89	0.03	-0.00	0.08*
N1	4	beech	8	130	0.63 ± 0.08***	-0.22 ± 0.08**	0.79	0.88	-0.00	0.02	0.29***
N1				130	1.02 ± 0.03***	-0.07 ± 0.07	0.90	0.91	0.01	0.01	0.00
N2	1	beech	53	97	1.31 ± 0.08***	0.23 ± 0.16	0.83	0.83	-0.01	-0.00	0.03
N2	2	beech	49	97	1.64 ± 0.09***	-0.06 ± 0.18	0.87	0.88	0.00	-0.00	-0.01
N2	3	beech	10	97	0.68 ± 0.04***	-0.11 ± 0.05*	0.89	0.82	0.01	0.00	-0.00
N2	4	beech	8	97	0.51 ± 0.08***	-0.14 ± 0.08	0.80	0.78	-0.01	0.00	0.26**
N2				97	1.04 ± 0.06***	-0.02 ± 0.11	0.87	0.88	-0.00	-0.01	0.02
S1	1	beech	43	130	0.81 ± 0.08***	-0.23 ± 0.10*	0.77	0.80	-0.01	0.01	0.34**
S1	2	oak	40	130	0.26 ± 0.01***	-0.10 ± 0.02***	0.92	0.94	0.05*	0.01	-0.01
S1	3	beech	39	97	0.39 ± 0.12**	-0.14 ± 0.12	0.64	0.81	0.01	0.01	0.40***
S1	4	beech	46	130	0.40 ± 0.05***	-0.13 ± 0.06*	0.76	0.87	-0.01	0.01	0.40***
S1				130	0.49 ± 0.05***	-0.17 ± 0.06**	0.80	0.84	-0.01	0.00	0.30**
S3	1	beech	45	124	0.52 ± 0.06***	-0.22 ± 0.07***	0.83	0.86	-0.01	0.02	0.22***
S3	2	beech	39	124	0.86 ± 0.08***	-0.35 ± 0.10***	0.84	0.90	-0.00	-0.00	0.09*
S3				124	0.69 ± 0.07***	-0.28 ± 0.08***	0.84	0.87	-0.01	0.01	0.12*

files show significant slopes b_{RWU} (Table S3 in the Supplement), which reveals a significant linear relationship with E_{opt}. The profile-based results also highlight that there is considerable within-site variability of the response of E_{RWU} to E_{opt}, with significant slopes ranging between 0.15 and 1.17. Testing the regression residuals for an influence of soil moisture content we find 10 of 16 forest soil profiles with significant residual correlation R^2_θ. At the grass site two profiles showed even larger residual correlations to θ than to E_{opt} ($R^2_\theta = 0.71, 0.72$). Testing for additional correlation of VPD and wind speed on the regression residuals of E_{RWU} to E_{opt} we find that VPD has generally low additional value with only three profiles with significant influences. Wind speed shows significant residual correlation at 3 out of 16 profiles. Root water uptake at a specific sensor level ($E_{\mathrm{RWU},d,z}$) allows one to assess at which depths plant water extraction and/or capillary rise due to soil evaporation are effective. E_{RWU} is detected at almost all soil moisture sensors during the growing season in 2013 (Fig. S4 in the Supplement). However, E_{RWU} at the deepest sensor is much lower than what is observed at the top (0–20 cm) soil layer. Comparing the grass site (G1) with the forest sites we find that the grass site has much larger E_{RWU} from the top-layer (0–20 cm)

than from deeper layers. Further, we can see that the top-layer uptake decreases during the drier summer period July to September. The reduction is the strongest at the grass site, whereas the forest sites show a more evenly distributed uptake with soil depth.

3.4 Influence of topography and stand structure

The results show that most of the daily variability in both transpiration estimates is driven by atmospheric demand. The slope of the linear regression of E_{sap}, SFD, and E_{RWU} to E_{opt} provides a summary statistic of how strong a site or a tree responds to atmospheric demand. In the following we evaluate which location factors correlate with the slopes of the linear regressions. We concentrate on topographic and stand structural parameters.

The most obvious factor is the aspect of the sites. While b_{sap} does not show aspect-related differences, we find that b_{SFD} and b_{RWU} are higher at the north-facing sites and lower at the south-facing sites. This is found at the site-average level (Table 2), at the soil profile level (Table S3 in the Supplement) and at the tree level (Table 3). The differences are, however, only significant for b_{SFD} at the tree level being larger at the north-facing slope with average $b_{\mathrm{SFD}} = 1.03$

Table 4. Site topographic characteristics with average inclination of each site is given in column "slope angle". Column, $R_{g,c}$ is the average global radiation $R_{g,c}$, and E_{opt} and E_{PM} are all averaged for the vegetation period 10 June–20 October. Values of site G1 are measured directly, values of the forested sites are estimated by the topographic correction of solar radiation.

Site	Slope angle (°)	$R_{g,c}$ (W m^{-2})	E_{opt} (mm d^{-1})	E_{PM} (mm d^{-1})
N1	14	153	1.46	2.19
N2	18	148	1.41	2.15
S3	30	192	1.82	2.44
S2	22	190	1.80	2.43
S1	24	191	1.81	2.44
G1	8	173	1.65	2.33

than at the south-facing slope $b_{SFD} = 0.63$, which is significant at the 0.05 level with a Student's t test.

Another topographic factor influencing the response to atmospheric demand is the inclination of the sites, where we find that the steeper the site the lower the slope of the linear regression of SFD to E_{opt} (cf. Tables 3 and 4). Both aspect and inclination affect the received solar radiation. According to the topographic correction of solar radiation, the north-facing sites received about 85 to 89 % of the solar radiation, which was observed at the grass site. In contrast the south-facing sites received about 108–110 %; see Table 4. This difference is confirmed by observations of air temperature within the forest, which reveal the same ranking across the sites as $R_{g,c}$.

Apart from the topographic data, the stand structure varies remarkably (see Table 5). At the two north-facing sites we find much understorey (> 98 % of trees smaller than DBH 15 cm) and a few tall trees, but no medium-sized trees between 15 and 50 cm DBH. The tall, dominant trees therefore have a well-lit canopy. The taller young trees form a secondary, lower but closed canopy layer. In contrast the south-facing sites S1 and S2 have about 20 medium sized trees per 20 by 20 m plot mainly between 16 and 65 cm DBH. These sites form a rather closed one-layer forest canopy. The valley site shows the largest tree size diversity with small, medium, and very tall trees. The stand composition differences of the sites result in quite different stand basal areas and thus total stand sapwood areas, which is the key factor in extrapolating SFD to site level. Although most trees are found at the north-facing sites, their total sapwood area is about half of the south-facing sites. The valley site (S3) has the largest sapwood area (Table 5). The LAI measurements also show the largest values for the valley site and slightly lower values for the south-facing site. Lower values are found at the north-facing sites. However, the differences in LAI between sites are comparably small when compared with sapwood area.

Plotting b_{SFD} as a function of the site-average sapwood area per tree (A_s / n_{tree}) (see Fig. 6), we find that b_{SFD} de-
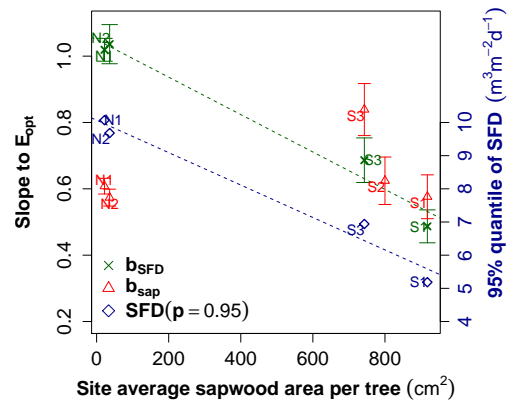

Figure 6. Sensitivity to E_{opt} as a function of the site-average sapwood area per tree computed by A_s / n_{tree}. On the left y axis: sensitivity of site-average sap flux density b_{SFD} (green crosses; see also Table 3) and the sensitivity of the upscaled transpiration estimate b_{sap} (red triangles). The vertical bars show the standard deviation of the sensitivity estimates tabulated in Tables 2 and 3. Right y axis: 95 % quantile of daily SFD maxima per site to estimate a robust maximum SFD. The dashed lines show linear regression model fits.

creases with A_s / n_{tree}. In addition, the maximum SFD estimated as the 95 % quantile of the daily maxima show a very similar decline. Thus, both measures show higher sap flux densities in the younger and smaller north-facing stands as compared to the older south-facing stands. In contrast the sensitivity of E_{sap} is rather constant $b_{sap} \approx 0.6$ [mm d^{-1}] / [mm d^{-1}] across sites at the hillslopes. Only at the valley site b_{sap} is significantly higher with ≈ 0.8 [mm d^{-1}] / [mm d^{-1}]. Although this site has a lower sapwood area per tree (A_s / n_{tree}) than the upper south-facing sites, the total sapwood area at S3 is larger, because of a few very tall trees; see Table 5.

4 Discussion

4.1 Using thermodynamic limits to estimate daily potential evaporation

Generally, there are two different physical limitations of atmospheric evaporative demand, which have been used for modeling E, (i) by energy limitation, and (ii) the mass exchange limitations, which requires that the vapor is removed before it might condense again (Brutsaert, 1982). The approach of maximum convective power applied here combines both of these physical constraints and emphasizes the strong link between the energy balance and the strength of convective motion.

The maximum power-derived estimate of potential evaporation E_{opt} is quite similar to the Priestley–Taylor formulation, but has two key differences. First, the Priestley–Taylor equation contains an additional empirical factor, which has been interpreted as an effect of large-scale advection or

Table 5. Observed biometric characteristics of the five forested sites along the transect. Column names: n_{tree} ... number of trees with circumference > 4 cm in a 20 by 20 m reference plot, diameter at breast height (DBH) distribution with minimum, first quartile, mean, third quartile, and maximum (cm), total stand basal area A_b (m^2 ha^{-1}), total stand sapwood area estimated from published allometric relationships A_s (m^2 ha^{-1}); see Sect. 2.4. Site leaf area index (LAI) was derived from the difference of summer LAI$_s$ and winter LAI$_w$.

| site | n_{tree} | DBH (cm) | | | | | A (m^2 ha^{-1}) | | LAI (m^2 m^{-2}) | | |
		min	Q25	mean	Q75	max	A_b	A_s	LAI$_s$	LAI$_w$	LAI
N1	346	< 1.3	2.1	3.8	4.4	65.4	25	19	7.5	2.3	5.2
N2	196	< 1.3	1.6	4.1	4.0	66.5	29	18	7.5	1.7	5.9
S3	28	1.8	12.7	30.2	40.7	80.9	75	52	8.1	1.7	6.5
S2	20	19.1	32.4	37.4	44.5	63.8	60	40	7.4	1.2	6.3
S1	17	16.4	31.8	41.1	49.8	58.9	61	39	7.1	0.7	6.4

boundary layer dynamics (Brutsaert, 1982). The second difference is the use of net shortwave radiation in our model, as opposed to net radiation in the Priestley–Taylor equation, the latter of which is not an independent forcing, as it depends on the surface temperature. Using shortwave radiation has important practical advantages because R_{sn} can be obtained from global radiation measurements and albedo information. Further topographic influences on incoming radiation can be directly computed by topographic radiation correction methods (Šúri and Hofierka, 2004). This also circumvents the necessity of collecting site-specific radiation data, which can be challenging above high vegetation like forests.

The derivation of E_{opt} is based on a representation of an atmosphere, which is in equilibrium with the underlying surface and the surface–atmosphere exchange of heat, moisture, and momentum is driven by locally absorbed solar radiation (Kleidon and Renner, 2013b). This implies that meteorological variables such as wind speed or vapor pressure deficit, which are commonly used in Penman formulations, cannot change independently, but are rather constrained by land–atmosphere interaction. In order to test if these assumptions are generally met, we tested for the effect of VPD on transpiration in our data set. The results showed that VPD and wind speed did not add consistently to the explained variance. In addition the correlation of the transpiration estimates to the FAO Penman–Monteith grass reference evaporation is on average slightly higher but follows the same patters across sites. Hence, the two additional input variables only slightly increased the predictability of atmospheric demand, which is consistent with the residual regression analysis above. Both of these results indicate that E_{opt}, which is a function of absorbed solar radiation and surface temperature only, captures the dominant drivers of daily sap velocity variations within this temperate forest without requiring further data on wind speed and VPD.

The dominance of absorbed solar radiation in explaining latent and sensible heat fluxes was also found by Best et al. (2015), who showed that simple linear regression models with solar radiation and temperature as input and thus without any information on wetness conditions had a similar performance than commonly used land-surface models at 20 di-

verse tower flux sites. However, an improved reproduction of sensible and latent heat fluxes was obtained by Best et al. (2015) when relative humidity was included into their regression model. It is likely that our potential evaporation estimate E_{opt} represents evaporation in a wet environment, whereas in drier environments, air humidity may become increasingly important. Interestingly, in contrast to our approach of eliminating air humidity while considering air temperature as an independent variable, Aminzadeh et al. (2016) estimated wet environment evaporation potential as a function of radiation and air humidity, while eliminating air temperature. Clearly, more investigations, encompassing larger and more diverse data sets, are needed to better understand general patterns of atmospheric control on transpiration. For example, it may well be that air humidity carries information about soil moisture and hence adds to explanatory power of transpiration models in water limited environments, while radiation represents the main control in energy-limited environments. In how far wind, air humidity, and temperature are affected by the land–atmosphere coupling and can hence be treated as internal variables, likely also depends on the scale of interest.

The derivation of E_{opt} shown in Sect. 2 was based on a range of simplifying assumptions to focus on the emerging maximum power limit in a coupled land–atmosphere system (Kleidon and Renner, 2013b; Kleidon et al., 2014). Most important features, which need to be addressed in future work are (i) changes in heat storage, (ii) a revision of the simplified scheme for longwave radiative exchange, and (iii) horizontal circulation patterns by large scale and mesoscale circulation. By assuming a steady state, heat storage effects were neglected in the derivation of the turbulent fluxes J_{opt}. However, heat storage in the surface–atmosphere system is an important mechanism to balance the seasonally and diurnally varying input of solar radiation. A comparison of $J_{opt} = R_{sn} / 2$ with the empirical net radiation estimate of Allen et al. (1998), which was used to estimate E_{PM} showed that J_{opt} is consistently lower during summer. Thus, to improve daily estimates based on thermodynamic limits, it is recommended to consider seasonal heat storage effects in the derivation. Heat storage is even more relevant at the diurnal timescale, which reduces the applicability of E_{opt} as given

in Eq. (5). The relevance of considering heat storage is illustrated in Fig. 7, which shows a distinct hysteresis of both sap flow and air temperature with respect to global radiation on a sunny day. Both sap flow and temperature linearly increase with shortwave radiation in the morning hours, but remain high after midday until sunset. Thus, for the same amount of received global radiation there is a distinct difference between morning and afternoon transpiration. While moisture storage in soil and plants also affect the hysteresis, the dominant magnitude of the hysteresis is probably due to the lag of temperature to radiation leading to a VPD-radiation lag (Zhang et al., 2014). Hence, for predictions at the diurnal timescale, heat storage effects as well as boundary layer dynamics have to be accounted for.

Another limitation of the approach is the simple linearized scheme for longwave heat exchange. The description of radiative exchange affects the maximum power limit, because longwave radiation "competes" with the convective fluxes to cool the surface (Kleidon et al., 2015). Although the parameter describing the net longwave radiative exchange drops out in the maximization for the convective fluxes, the radiation scheme affects the partitioning of radiative and convective fluxes at the surface. Therefore, a more detailed description of radiation transfer processes will increase the ability to predict surface energy partitioning.

The third limitation is concerned with the spatial representativity of E_{opt}, but also other potential evaporation formulations and the role of horizontal heat and mass exchange. While the land surface is generally quite heterogeneous, the lower atmosphere is mostly well mixed (Claussen, 1991). By using the topographically corrected incoming radiation we effectively treated each site as an independent surface–atmosphere column. We thus neglected any lateral fluxes that could alter the estimated potential evaporation. The topographic correction increased the potential evaporation at the south-facing and decreased estimates for the north-facing sites. To evaluate this effect with respect to the transpiration estimates, we used the global radiation measured at the nearby grassland site as forcing for all forest sites. The correlation to the transpiration estimates was unaffected, but the topographic correction slightly amplified the aspect-related differences of the response to E_{opt} between sites (Fig. S1 in the Supplement). For a better understanding of such microclimatic effects spatial observations of the canopy surface energy balance are required to test more detailed models, which include horizontal exchange processes. Progress in this respect will be quite important for the parameterization of subgrid processes in numerical land-surface models.

4.2 Topographical and stand composition effects

Our results demonstrate a strong influence of daily variations in atmospheric demand on both transpiration estimates. This strong correlation at the daily timescale may allow us to separate the timescales of atmospheric demand and plant water
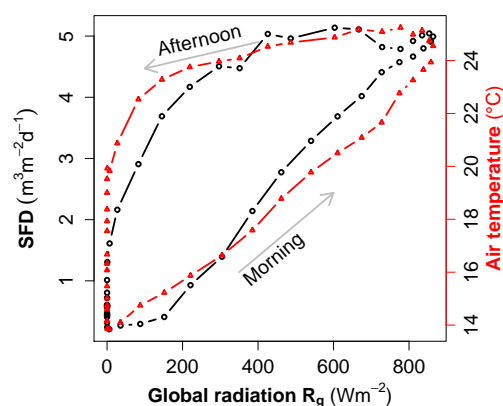

Figure 7. Hysteresis of sap flux density (left y axis) and air temperature (right y axis, red) plotted as a function of global radiation at the field site G1. Data are half-hourly values over one sunny summer day (7 July 2013). Sap flow data are taken from a beech (tree 1) at site S1.

limitations, which may become relevant at timescales larger than 1 day. Differences in the slope of the relationship to E_{opt} can then be compared across sites and be used to identify potential permanent site controls on transpiration.

Of the many factors that influence transpiration, stand composition and topography were the most important invariant controls during our measurement campaign. The measurement transect was placed on a valley cross section to primarily reveal the influence of hillslope aspect. Our results indicate only significant effects of aspect and hillslope angle for the sensitivity of SFD to E_{opt}, but no effects for the sensitivity of the upscaled transpiration estimate E_{sap}. E_{RWU} shows a weak relation to these topographic factors, which was, however, not significant because of the larger uncertainty of the soil moisture-based estimate.

The biometric measures of stand composition, however, also co-vary with aspect and hillslope inclination. Here we found a strongly negative linear relationship of b_{SFD} and the maximum sap flux densities to the site-average sapwood area per tree (Fig. 6). Such a decline in b_{SFD} and maximum SFD with sapwood area was found to be a universal tree hydraulic mechanism observed across different tree species (Andrade et al., 1998; Meinzer et al., 2001). Interestingly, Andrade et al. (1998) found that maximum sap velocity nonlinearly declined with sapwood area, with strongest effects at very small trees or branches with $A_s < 100\,\text{cm}^2$. Considering such an increase in b_{SFD} for the understorey vegetation at the north-facings sites in our study would increase their relevance in estimating stand transpiration.

In addition to the tree size differences, our sites show marked differences in canopy structure. The open canopy structure may explain the larger b_{SFD} of the dominant trees sampled at the north-facing sites, because tree growth could be enhanced by gaps in the canopy structure. For example Schweingruber et al. (2006) showed that annual tree

ring width of beech trees increase quickly after neighboring trees have been cut. At the south-facing sites average tree size is high but there is a low number of stems. Here individual tree growth is limited by the neighboring trees with similar demands for light, water, nutrients, and space. Self-thinning or thinning by forest management has resulted in a more even-sized stand structure with old and large trees. Thus, the closed canopy structure, which is composed of well-established trees, may have lead to a more conservative water use per tree, which is reflected by low b_{SFD} and low maximum sap flux densities. These arguments are consistent with results of studies that show higher sap flux densities of thinned forest stands as compared to control stands (Morikawa et al., 1986; Bréda et al., 1995; Nahm et al., 2006).

The upscaling procedure integrates both the tree distribution within the stand and the sap flux density observations to yield the stand transpiration estimate E_{sap}. Apparently this has led to a compensation of the vastly different stand structure and sap flux densities across sites. Due to this tradeoff between SFD and the sapwood area similar transpiration rates are achieved at the hillslope sites. Therefore, forest transpiration may indeed be regarded as a conservative hydrological process (Roberts, 1983) even in this very complex terrain. Only for the valley site S3 significantly larger E_{sap} and b_{sap} was estimated. This site has comparably high maximal SFD and the largest total sapwood area, even though A_s / n_{tree} is lower than observed at the upper south-facing sites. The most likely reason for the comparably dense, but tall forest is the vicinity to the nearby stream, which reduces potential soil water limitations. A similar upslope–downslope effect was recently also established by Kume et al. (2015) for a mountainous stand of Japanese cypress with the lower site having taller trees with higher SFD but same tree density.

4.3 Response to soil moisture

Due to low rainfall amounts, soil moisture decreased from July to September at all sites and all depths. Thus the soil moisture reduction may have limited transpiration. We captured this effect of soil moisture limitation of transpiration through the regression of the residuals of the transpiration to E_{opt} relationships to site-average soil moisture conditions. Results showed that soil moisture explained a significant part of the residuals of E_{sap} at the south-facing sites (Table 2), which implies that site-scale transpiration was also water limited during the dry period in August. At the north-facing sites water limitation at the site scale was only apparent during a shorter period in September. However, we found significant residual correlation to soil moisture at three of four sampled small beech trees. This suggests that small trees are more susceptible to water shortage.

We argue that soil water limitation effects on transpiration could be topographically enhanced. First, by an aspect that affects the amount of received solar radiation and thus the atmospheric demand for water. A higher atmospheric demand increases evaporation from intercepted water and from the soil, which reduces the amount of precipitation entering the soil. Second, the hillslope inclination could have enhanced lateral runoff at the steeper south-facing sites, which reduces the soil water holding capacity (Bronstert and Plate, 1997). These topographical factors of soil moisture availability are also apparent in the tree species composition of our sites. While the north-facing sites are predominantly composed of beech and a few spruce trees, the south-facing sites have about 10 % oak trees, which are known to cope well at more dry sites (Zapater et al., 2011).

4.4 Limitations of transpiration estimates

4.4.1 Limitations of sap flow observations

Generally, sap flow observations are not limited by spatial heterogeneity and complex terrain, which would limit the applicability of micrometeorological measurements (Wilson et al., 2001). Installation is relatively simple and sensors are inexpensive. Despite these advantages, we experienced the following limitations:

(a) Deriving water fluxes requires extrapolation from the point measurement at some specific place within the stem to the entire tree. However, sapwood conductivity can have radial and circumferential differences and species-specific properties (Wullschleger and King, 2000; Saveyn et al., 2008). This can easily bias sap flow estimates (Köstner et al., 1998; Shinohara et al., 2013; Vandegehuchte and Steppe, 2013). An indication of this problem is that we found different b_{SFD} at the same tree installed the year before. Comparison with measurements taken at the same trees from the previous year showed differences in b_{SFD} ranging between -0.39 and 0.23 with an average of 0.04 $[m^3 m^{-2} d^{-1}] / [mm\, d^{-1}]$ (estimated for nine trees with more than 30 days of data each year).

(b) There is a sample bias towards larger trees as the method is more difficult with very small trees, which would require a different type of sensor, because the heat ratio method is designed only for lower sap velocities (Marshall, 1958; Burgess et al., 2001). This adds a sampling uncertainty in estimating site transpiration where much understorey exists. This is especially relevant for the north-facing sites, with a median DBH of 4 cm. This means that most trees were not sampled. The sampling rather reflected the trees that contributed most to the stand sapwood area.

(c) The inter-comparison of sap flux density measured in different trees is limited by the fact that xylem characteristics in the estimation of SFD are required (Burgess

et al., 2001). Most important is the thermal diffusivity of sapwood, k_w as used in Eq. (A1). This conductivity is a function of wood density and wood water content m_c (Burgess et al., 2001; Vandegehuchte and Steppe, 2012a), both of which vary between species and trees (Gebauer et al., 2008). Xylem water content m_c, which in addition influences the apparent sap flux density through affecting the sapwood heat capacity (see Eq. 7), was shown to have seasonal changes in diffuse-porous species (Glavac et al., 1990; Hao et al., 2013). Glavac et al. (1990) found that m_c can reduce to about 25 % in sampled European beech trees during summer. Such a decline would thus reduce the apparent sap velocities. Therefore, it is recommended to use methods that take into account wood moisture content changes (Vandegehuchte and Steppe, 2012b). Here, in the absence of measurements of such wood properties we used the same parameters for all trees.

4.4.2 Limitations of root water uptake estimates from soil moisture variations

The advantage of using temporally highly resolved soil moisture readings is that it allows one to estimate root water uptake without further information on soil properties (Guderle and Hildebrandt, 2015). The accuracy of the method depends on various factors that can influence results:

(a) Data filtering: the method only applies under conditions with negligible soil water movement excluding events of infiltration, drainage, capillary rise, or hydraulic redistribution. These fluxes can have major influences on the observations of soil moisture and comprise the second term of the right-hand side of Eq. (A6). Thus, the estimates depend on the choice of suitable filter criteria. A very strict filter would reduce the number of estimates, whereas soft filter criteria may result in biased E_{RWU} estimates. Hence, seasonal or annual totals cannot be derived from this method alone. We use relatively strict filter criteria for nighttime fluxes of 0.1 Vol %, which is close to the sensor resolution. This filter criteria set the maximum accuracy per soil layer of 200 mm depth to 0.2 mm d^{-1}.

(b) Soil heterogeneities, dominant at the hillslopes, can induce large local variations in soil moisture and may lead to dissimilar / biased E_{RWU} compared to other methods (Wilson et al., 2001). Here, we found that the influence of E_{opt} and soil moisture content on E_{RWU} varied between soil profiles at a specific site (Table S3 and Fig. S5 in the Supplement). Large differences were observed at site N2, which results in a quite uncertain site-average estimate of E_{RWU}. Therefore, it is recommended to install several, representative measurement profiles when such a soil water budget method is

used for transpiration estimation in heterogeneous terrain (Schwärzel et al., 2009).

(c) Deep root water uptake in response to drying topsoil may cause root water uptake below the deepest measurement depth in forest sites as observed e.g. by Teskey and Sheriff (1996); Wilson et al. (2001). Observations from the deepest sensor profile confirm root uptake at 60 cm depth (Fig. S4 in the Supplement), which also persists during the dry period. However, overall the contribution of deep root water uptake is assumed to be small, given the low observed diurnal variations.

4.4.3 Upscaling sap flow to site-scale transpiration

The estimates of site-scale transpiration based on up-scaled sap flow measurements were of similar magnitudes and correlated well with estimates derived from soil moisture variations. The seasonal estimates by E_{sap} are about 50 mm lower than other estimates for beech forests. For example Schipka et al. (2005) found 200–300 mm per year for European beech forests in Germany. Their sites, however, have been located in less steep terrain.

The comparison between E_{RWU} and E_{sap} also revealed striking differences, which could be an indication of the potential shortcomings of both methods, as discussed above. While the south-facing sites are in good agreement, E_{sap} at the north-facing sites seems to be quite low. First, this is due to the low basal area at the north-facing site. One reason could be that the assumed sapwood area of the few tall trees is much larger than that reported in the literature. Another possible reason could be that small trees (< 8 cm DBH), which were not sampled, had a significant contribution to stand transpiration. Also E_{RWU} might overestimate actual transpiration because soil evaporation would equally contribute to the diurnal signal in soil moisture. For example Bréda et al. (1993) also found consistently larger estimates of a soil water balance method than stand transpiration estimates, which was attributed to soil evaporation by the authors.

5 Summary and conclusions

We aimed to infer the dominant temporal and spatial controls on forest transpiration along a steep valley cross section through ecohydrological measurements of sap flow and soil moisture and their relation to atmospheric evaporative demand. The estimation of transpiration in space and time for forests in complex terrain is a challenge in its own right. Obtaining transpiration is only possible through indirect observations, whereby each method has its own limitations. Therefore, we used two independent observations to obtain site-scale estimates of transpiration along the hillslope transect. To estimate atmospheric demand, a formulation similar to the well-known Priestley–Taylor equilibrium evaporation concept was employed. The formulation is based on

a simplified energy balance representation of the surface–atmospheric system and hypothesizing that convection operates at its upper thermodynamic limit. The formulation does not require empirical parameters and only requires data on the absorbed solar radiation and temperature. We find that at the daily timescale this approach explains most of variability in both transpiration estimates at the site and tree scale. This suggests that atmospheric demand is the dominant control on daily transpiration rates in this temperate forest. Although the well-established FAO Penman–Monteith reference evaporation yields slightly higher correlation and 20–30 % higher values, it requires additional data of net radiation, VPD and wind speed. Thereby both, VPD and wind speed did not add consistently to the explained variance and are also difficult to obtain above forests. While our results demonstrate that thermodynamic limits provide a first-order estimate for potential evaporation, we have to stress that the derivation is based on the simplest possible energy balance representation. Further refinements will probably improve the predictability of surface exchange fluxes.

Despite the prevailing topographic contrasts between the north-facing and the south-facing measurement sites, we find that up-scaled stand transpiration yields rather similar seasonal totals as well as a similar average response to atmospheric demand. This similarity is achieved through a compensation of the low sapwood area with high sap flux densities at the north facing sites, while at the south-facing sites a high sapwood area was accompanied with low sap flux densities. It appears that individual and stand average sap flux densities can vary strongly in heterogeneous terrain in order to compensate for tree size and stand structural differences through tree hydraulic mechanisms. The importance of these stand structural differences on stand transpiration thus masks the potential effects of topographical factors such as aspect and hillslope angle, which are cross correlated. However, during dry periods we find that topographic factors can enhance the response of transpiration to soil water limitation.

Despite unavoidable limitations in estimating stand transpiration and potential evaporation in complex terrain, we find that relating the employed ecohydrological observations to a thermodynamically constrained estimate of atmospheric demand enables important insights in the temporal drivers of transpiration and how they vary at the hillslope scale. First our results highlight the dominance of absorbed solar radiation as the main and independent driver of land–atmosphere exchange. Second, our results suggest an intriguing interplay of tree hydraulics and stand composition, which seemingly leads to transpiration rates close to its physical limits. We conclude that this approach should help us to better understand surface–atmosphere coupling in relation to thermodynamic constraints and how vegetation adapts to these.

Appendix A: Detailed description of transpiration estimates

A1 Measurement and correction of heat pulse velocity

We used sap flow sensors based on the heat ratio method (Burgess et al., 2001). Thereby three needles with equal distance are vertically inserted into the tree. The upper and lower needles measure the change in temperature after a short heat pulse was emitted by a heating element in the middle needle. The heat pulse velocity v_h is proportional to the logarithmic ratio of the temperature differences measured before and at t_1 usually 60 s after the heat pulse at the lower (ΔT_{dn}) and upper (ΔT_{up}) needles (Marshall, 1958; Burgess et al., 2001):

$$v_h = \frac{4 k_w t_1 \log \frac{\Delta T_{up}}{\Delta T_{dn}} - x_2^2 + x_1^2}{2 t_1 (x_1 - x_2)}, \tag{A1}$$

whereby k_w is the thermal diffusivity of the xylem, and x_1 and x_2 are the vertical distances to the heater. The sensors have the standard distance of 0.6 cm. This distance can easily be slightly shifted during the installation into living trees, which causes a systematic bias. This sensor alignment bias can be corrected when sap flow is zero (Burgess et al., 2001). Setting $v_h = 0$ and rearranging Eq. (A1), we can estimate the distance of the upper needle x_1 while assuming $x_2 = 0.6$:

$$x_1 = \sqrt{x_2^2 - 4 k_w t_1 \log \frac{\Delta T_{up}}{\Delta T_{dn}}}. \tag{A2}$$

We prefer Eq. A2 over the published correction in Burgess et al. (2001) because it allows to correct for both, positive and negative nighttime biases in heat velocities. We estimated the corrected distance x_1 by assuming zero flow during nighttime between 01:00 and 04:00 LT and the median of x_1 for the whole installation period. The installation of the sensor needles injures the surrounding xylem vessels and reduces the actual sap flow around the sensor. We applied a polynomial wounding correction $v_c = b\, V_h + c\, V_h^2 + d\, V_h^3$ with wounding correction parameters $b = 1.8558$, $c = -0.0018$, and $d = 0.003$, applicable for a sensor spacing of 0.6 cm and a drilling hole size of 2 mm, which is tabulated in Burgess et al. (2001).

A2 Upscaling of sap flow

The needles measure heat-pulse velocities at depths of 5, 18, and 30 mm within the stem. Following the user's manual we assigned for each sensor depth a representative radius of 15, 25, and 40 mm below the cambium radius r_x, which is obtained by assuming that the cambium takes 1 % of the total radius, thus $r_x = 0.99 \cdot \text{DBH} / 2$.

Because tall trees may have a wider active xylem depth than measured by the inserted sap flow needles (Gebauer

et al., 2008), we derived three different estimates of the representative sapwood area of the innermost sensor, which provides the range and a best-guess estimate. A minimal estimate is obtained by assuming a representative annulus of 15 mm depth for the sensor and zero flow in the inner sapwood, which is calculated by $A_{S3,min}$. Assuming that sap flux density remains constant at the innermost sensor level throughout the inner sapwood area provides a maximal estimate of sap flux. Most realistic is the assumption of a linear decline reaching no flow at the estimated heartwood radius $A_{S3,lin}$ similar to Pausch et al. (2000):

$$A_{S3,min} = \pi \left((r_x - 25\,\text{mm})^2 - (r_x - 40\,\text{mm})^2 \right), \tag{A3}$$

$$A_{S3,lin} = \pi \left((r_x - 25\,\text{mm})^2 - \frac{1}{3} \left((r_x - 25\,\text{mm})^2 \right.\right.$$
$$\left.\left. + (r_x - 25\,\text{mm})\, r_h + r_h^2 \right) \right), \tag{A4}$$

$$A_{S3,max} = \pi \left((r_x - 25\,\text{mm})^2 - (r_x - r_h)^2 \right). \tag{A5}$$

Stem sapwood area was computed using published allometric power-law relationships of the form $A_s = a\, \text{DBH}^b$. For beech and alder we used the relationship published in Gebauer et al. (2008), for oak we used Schmidt (2007) and Alsheimer et al. (1998) for spruce. Then the radius of the heartwood r_h is obtained from sapwood area estimates. For small trees with radius smaller than the representative annulus depth we set the area to 0.

A3 Root water uptake estimation

The soil water continuity equation at a point in the soil may be written as Cuenca et al. (1997):

$$\frac{\partial \theta}{\partial t} = -\frac{\partial q_i}{\partial x_i} + S, \tag{A6}$$

where θ is the soil moisture content, q summarizes any soil water fluxes over an orthogonal coordinate system x_i with horizontal (x, y) and vertical directions (z). The sink term S is the root water uptake, which when integrated over the soil volume V_s yields the transpiration flux E_{RWU} (Cuenca et al., 1997):

$$E_{RWU} = \int_{V_s} S\, dV_s = \int_{V_s} \frac{\partial \theta}{\partial t} dV_s + \int_{V_s} \frac{\partial q_i}{\partial x_i} dV_s. \tag{A7}$$

Hence, to estimate E_{RWU} we need to resolve the two terms in Eq. (A7). The first term is the temporal evolution of soil moisture, which is in principle measured by the soil moisture sensors. The second term describes soil water fluxes within the soil such as downward fluxes during an infiltration event. The soil water fluxes q_i themselves depend on soil moisture, through its role in determining soil water potentials and unsaturated hydraulic conductivity. Soils along hillslopes have large spatial heterogeneity of their hydraulic properties and
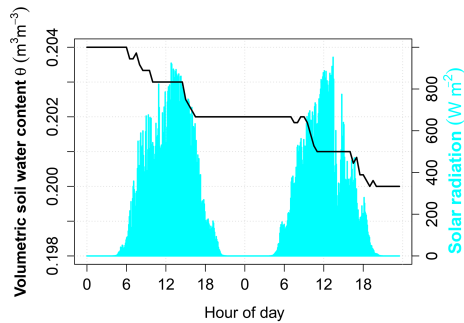
Figure A1. Observed diurnal decline in soil moisture over two sunny days in summer 2013 to illustrate the approach to estimate daily root water uptake from diurnal soil moisture variations. E_{RWU} is estimated at sensor level per day as a cumulative sum of differences from sunrise to sunset, in the absence of any nighttime variations or daytime increases in soil moisture.

pose many influences on the second term of Eq. (A7), which makes continuous estimation of root water uptake difficult.

There are, however, periods and locations where soil water fluxes q_i, such as drainage, capillary rise, etc., are of minor importance. Especially during dry conditions the reduction of soil moisture is dominated by root water uptake and soil evaporation during daytime, as illustrated in Fig. A1. Under these radiation-driven conditions, we observe rather constant nighttime moisture levels, which thus indicates that soil water fluxes are not active and nocturnal root–soil exchange is negligible. Thus, nighttime soil moisture dynamics are a practical filter to exclude days with dominant drainage or capillary rise fluxes. To estimate daily root water uptake we use soil moisture observations on a half-hourly basis. We first quantify the daytime change in soil moisture per sensor $\Delta\theta_{d,s}$ by cumulative sum of differences of soil moisture (at 30 min intervals) from astronomical sunrise to sunset:

$$\Delta\theta_{d,s} = \sum_{t=t_{sunrise}}^{t=t_{sunset}} (\theta_{t+1} - \theta_t). \tag{A8}$$

Assuming that the sensor observation is representative for the respective soil depth Δz of the sensor, we obtain a flux estimate $E_{RWU,d,z} = -\Delta\theta_{d,s}\Delta z$ per soil layer. A constant soil depth of $\Delta z = 200\,\text{mm}$ per sensor level was assumed for all soil profiles. We then summed up the contributions $E_{RWU,d,z}$ of each soil layer to obtain a daily root water uptake $E_{RWU,d}$ per profile. For most profiles this allowed us to estimate $E_{RWU,d}$ down to a depth of 600 mm, and for three profiles down to 800 mm (see Table S1 for an overview of sensor placement). During sensor installation thick roots were mostly found until a depth of $\approx 300\,\text{mm}$ with sporadic fine roots up to 800 mm depth.

The data were filtered for (i) precipitation (daily sum < 0.1 mm and rainfall of previous day < 1 mm), (ii) only negative daytime soil moisture changes $\Delta\theta_{d,s}$, and (iii) absolute cumulative nighttime changes in soil moisture $|\Delta\theta_{n,s}| < 0.1$ Vol %. Approximately 30 % of the actual data were retained, with details listed in Table S2 in the Supplement. Generally, diurnal variations of soil moisture are large in the upper soil depths compared to deeper layers. Thus, for estimating the total profile root water uptake, the upper sensors are very important. Unfortunately, we had to face sensor failure of top soil sensors at site N1, profile 2 and site S1 profiles 2 and 3; see Table S2 in the Supplement for an overview of available data. At these soil profiles we used the root water uptake estimates from the 2nd sensor level to fill the missing data. Two profiles, one at G1 and another at N2 were completely disregarded for site averaging due to sensor failures. The site-average was obtained from at least two profile-based E_{RWU} estimates. At the grass site this condition was relaxed because there were only a few days where E_{RWU} could be estimated from both profiles. At these few days the estimates of the two profiles were comparable.

The Supplement related to this article is available online at doi:10.5194/hess-20-2063-2016-supplement.

References

Allen, R., Pereira, L., Raes, D., and Smith, M.: Crop evapotranspiration-Guidelines for computing crop water requirements-FAO Irrigation and drainage paper 56, FAO, Rome, 300, 6541, 1998.

Alsheimer, M., Kästner, B., Falge, E., and Tenhunen, J. D.: Temporal and spatial variation in transpiration of Norway spruce stands within a forested catchment of the Fichtelgebirge, Germany, Ann. Sci. Forest Res., vol. 55, 103–123, EDP Sciences, 1998.

Aminzadeh, M., Roderick, M. L., and Or, D.: A generalized complementary relationship between actual and potential evaporation defined by a reference surface temperature, Water Resour. Res., 52, 385–406, doi:10.1002/2015WR017969, 2016.

Andrade, J. L., Meinzer, F. C., Goldstein, G., Holbrook, N. M., Cavelier, J., Jackson, P., and Silvera, K.: Regulation of water flux through trunks, branches, and leaves in trees of a lowland tropical forest, Oecologia, 115, 463–471, doi:10.1007/s004420050542, 1998.

Bachmair, S. and Weiler, M.: New Dimensions of Hillslope Hydrology, in: Forest Hydrology and Biogeochemistry, edited by: Levia, D. F., Carlyle-Moses, D., and Tanaka, T., vol. 216, 455–481, Springer Netherlands, Dordrecht, 2011.

Baumgartner, A.: Gelände und Sonnenstrahlung als Standortfaktor am Gr. Falkenstein (Bayerischer Wald), Forstwissenschaftliches Centralblatt, 79, 286–297, doi:10.1007/BF01815008, 1960.

Best, M. J., Abramowitz, G., Johnson, H. R., Pitman, A. J., Balsamo, G., Boone, A., Cuntz, M., Decharme, B., Dirmeyer, P. A., Dong, J., Ek, M., Guo, Z., Haverd, V., van den Hurk, B. J. J., Nearing, G. S., Pak, B., Peters-Lidard, C., Santanello, J. A., Stevens, L., and Vuichard, N.: The Plumbing of Land Surface Models: Benchmarking Model Performance, J. Hydrometeorol., 16, 1425–1442, doi:10.1175/JHM-D-14-0158.1, 2015.

Bohren, C. F. and Albrecht, B. A.: Atmospheric thermodynamics, Atmospheric thermodynamics, New York, Oxford, Oxford University Press, ISBN: 0195099044, 1, 1998.

Bonan, G. B.: Forests and Climate Change: Forcings, Feedbacks, and the Climate Benefits of Forests, Science, 320, 1444–1449, doi:10.1126/science.1155121, 2008.

Breña Naranjo, J. A., Weiler, M., and Stahl, K.: Sensitivity of a data-driven soil water balance model to estimate summer evapotranspiration along a forest chronosequence, Hydrol. Earth Syst. Sci., 15, 3461–3473, doi:10.5194/hess-15-3461-2011, 2011.

Bronstert, A. and Plate, E. J.: Modelling of runoff generation and soil moisture dynamics for hillslopes and micro-catchments, J. Hydrol., 198, 177–195, doi:10.1016/S0022-1694(96)03306-9, 1997.

Brutsaert, W.: Evaporation into the Atmosphere, Springer Netherlands, Dordrecht, 1982.

Bréda, N., Cochard, H., Dreyer, E., and Granier, A.: Water transfer in a mature oak stand (Quercuspetraea): seasonal evolution and effects of a severe drought, Canad. J. For. Res., 23, 1136–1143, doi:10.1139/x93-144, 1993.

Bréda, N., Granier, A., and Aussenac, G.: Effects of thinning on soil and tree water relations, transpiration and growth in an oak forest (Quercus petraea (Matt.) Liebl.), Tree Physiol., 15, 295–306, doi:10.1093/treephys/15.5.295, 1995.

Burgess, S. S. O., Adams, M. A., Turner, N. C., Beverly, C. R., Ong, C. K., Khan, A. A. H., and Bleby, T. M.: An improved heat pulse method to measure low and reverse rates of sap flow in woody plants, Tree Physiol., 21, 589–598, doi:10.1093/treephys/21.9.589, 2001.

Calder, I. R.: Water use by forests, limits and controls, Tree Physiol., 18, 625–631, doi:10.1093/treephys/18.8-9.625, 1998.

Claussen, M.: Estimation of areally-averaged surface fluxes, Bound.-Lay. Meteorol., 54, 387–410, doi:10.1007/BF00118868, 1991.

Cuenca, R. H., Stangel, D. E., and Kelly, S. F.: Soil water balance in a boreal forest, J. Geophys. Res.-Atmos., 102, 29355–29365, doi:10.1029/97JD02312, 1997.

de Bruin, H. A. R., Trigo, I. F., Bosveld, F. C., and Meirink, J. F.: A Thermodynamically Based Model for Actual Evapotranspiration of an Extensive Grass Field Close to FAO Reference, Suitable for Remote Sensing Application, J. Hydrometeorol., 17, 1373–1382, doi:10.1175/JHM-D-15-0006.1, 2016.

Dowle, M., Short, T., Lianoglou, S., and Srinivasan, A.: data. table: Extension of data. frame. R package version 1.9.4, 2014.

Famiglietti, J. S., Rudnicki, J. W., and Rodell, M.: Variability in surface moisture content along a hillslope transect: Rattlesnake Hill, Texas, J. Hydrol., 210, 259–281, doi:10.1016/S0022-1694(98)00187-5, 1998.

Farquhar, G. D., Caemmerer, S. v., and Berry, J. A.: A biochemical model of photosynthetic CO2 assimilation in leaves of C3 species, Planta, 149, 78–90, doi:10.1007/BF00386231, 1980.

Federer, C. A.: Forest Transpiration Greatly Speeds Streamflow Recession, Water Resour. Res., 9, 1599–1604, 1973.

Gebauer, T., Horna, V., and Leuschner, C.: Variability in radial sap flux density patterns and sapwood area among seven co-occurring temperate broad-leaved tree species, Tree Physiol., 28, 1821–1830, doi:10.1093/treephys/28.12.1821, 2008.

Glavac, V., Koenies, H., and Ebben, U.: Auswirkung sommerlicher Trockenheit auf die Splintholz-Wassergehalte im Stammkörper

der Buche (Fagus sylvatica L.), Holz als Roh- und Werkstoff, 48, 437–441, doi:10.1007/BF02627628, 1990.

Guderle, M. and Hildebrandt, A.: Using measured soil water contents to estimate evapotranspiration and root water uptake profiles – a comparative study, Hydrol. Earth Syst. Sci., 19, 409–425, doi:10.5194/hess-19-409-2015, 2015.

Haas, E., Klatt, S., Frählich, A., Kraft, P., Werner, C., Kiese, R., Grote, R., Breuer, L., and Butterbach-Bahl, K.: LandscapeD-NDC: a process model for simulation of biosphere-atmosphere-hydrosphere exchange processes at site and regional scale, Landsc. Ecol., 28, 615–636, doi:10.1007/s10980-012-9772-x, 2013.

Hao, G.-Y., Wheeler, J. K., Holbrook, N. M., and Goldstein, G.: Investigating xylem embolism formation, refilling and water storage in tree trunks using frequency domain reflectometry, J. Exp. Bot., 64, 2321–2332, doi:10.1093/jxb/ert090, 2013.

Holst, J., Grote, R., Offermann, C., Ferrio, J. P., Gessler, A., Mayer, H., and Rennenberg, H.: Water fluxes within beech stands in complex terrain, Int. J. Biometeorol., 54, 23–36, doi:10.1007/s00484-009-0248-x, 2010.

Holst, T., Rost, J., and Mayer, H.: Net radiation balance for two forested slopes on opposite sides of a valley, Int. J. Biometeorol., 49, 275–284, doi:10.1007/s00484-004-0251-1, 2005.

Ivanov, V. Y., Bras, R. L., and Vivoni, E. R.: Vegetation-hydrology dynamics in complex terrain of semiarid areas: 2. Energy-water controls of vegetation spatiotemporal dynamics and topographic niches of favorability, Water Resour. Res., 44, W03430, doi:10.1029/2006WR005595, 2008.

Jasechko, S., Sharp, Z. D., Gibson, J. J., Birks, S. J., Yi, Y., and Fawcett, P. J.: Terrestrial water fluxes dominated by transpiration, Nature, 496, 347–350, doi:10.1038/nature11983, 2013.

Juilleret, J., Iffly, J. F., Pfister, L., and Hissler, C.: Remarkable Pleistocene periglacial slope deposits in Luxembourg (Oesling): pedological implications and geosite potential, Bull. Soc. Nat. Luxembour., 112, 125–130, 2011.

Kleidon, A. and Renner, M.: A simple explanation for the sensitivity of the hydrologic cycle to surface temperature and solar radiation and its implications for global climate change, Earth Syst. Dynam., 4, 455–465, doi:10.5194/esd-4-455-2013, 2013a.

Kleidon, A. and Renner, M.: Thermodynamic limits of hydrologic cycling within the Earth system: concepts, estimates and implications, Hydrol. Earth Syst. Sci., 17, 2873–2892, doi:10.5194/hess-17-2873-2013, 2013b.

Kleidon, A., Renner, M., and Porada, P.: Estimates of the climatological land surface energy and water balance derived from maximum convective power, Hydrol. Earth Syst. Sci., 18, 2201–2218, doi:10.5194/hess-18-2201-2014, 2014.

Kleidon, A., Kravitz, B., and Renner, M.: The hydrological sensitivity to global warming and solar geoengineering derived from thermodynamic constraints, Geophys. Res. Lett., 42, 138–144, doi:10.1002/2014GL062589, 2015.

Kondratyev, K. Y. and Fedorova, M. P.: Radiation regime of inclined surfaces, Solar Energy, 1, 36–61, 1977.

Kume, T., Tsuruta, K., Komatsu, H., Shinohara, Y., Katayama, A., Ide, J., and Otsuki, K.: Differences in sap flux based stand transpiration between upper and lower slope positions in a Japanese cypress plantation watershed, Ecohydrology, doi:10.1002/eco.1709, 2015.

Köstner, B., Granier, A., and Cermák, J.: Sapflow measurements in forest stands: methods and uncertainties, Ann. For. Sci., 55, 13–27, doi:10.1051/forest:19980102, 1998.

Lee, R. and Baumgartner, A.: The Topography and Insolation Climate of a Mountainous Forest Area, For. Sci., 12, 258–267, 1966.

Lüttschwager, D. and Remus, R.: Radial distribution of sap flux density in trunks of a mature beech stand, Ann. For. Sci., 64, 431–438, doi:10.1051/forest:2007020, 2007.

Makkink, G.: Testing the Penman formula by means of lysimeters, J. Inst. Water Eng, 11, 277–288, 1957.

Marshall, D. C.: Measurement of Sap Flow in Conifers by Heat Transport. 1, Plant Physiol., 33, 385–396, 1958.

Meinzer, F. C., Goldstein, G., and Andrade, J. L.: Regulation of water flux through tropical forest canopy trees: Do universal rules apply?, Tree Physiol., 21, 19–26, doi:10.1093/treephys/21.1.19, 2001.

Miller, G. R., Chen, X., Rubin, Y., Ma, S., and Baldocchi, D. D.: Groundwater uptake by woody vegetation in a semiarid oak savanna: GROUNDWATER UPTAKE IN AN OAK SAVANNA, Water Resour. Res., 46, W10503, doi:10.1029/2009WR008902, 2010.

Monteith, J. L.: Evaporation and environment, Symposia of the Society for Experimental Biology, 19, 205–234, 1965.

Morikawa, Y., Hattori, S., and Kiyono, Y.: Transpiration of a 31-year-old Chamaecyparis obtusa Endl. stand before and after thinning, Tree Physiol., 2, 105–114, doi:10.1093/treephys/2.1-2-3.105, 1986.

Nahm, M., Holst, T., Matzarakis, A., Mayer, H., Rennenberg, H., and Geßler, A.: Soluble N compound profiles and concentrations in European beech (Fagus sylvatica L.) are influenced by local climate and thinning, Eur. J. For. Res., 125, 1–14, doi:10.1007/s10342-005-0103-5, 2006.

Newey, W. K. and West, K. D.: Automatic Lag Selection in Covariance Matrix Estimation, Rev. Econ. Stud., 61, 631–653, 1994.

Oke, T.: Boundary layer climates, Routledge, London and New York, 1987.

Ozawa, H., Ohmura, A., Lorenz, R. D., and Pujol, T.: The second law of thermodynamics and the global climate system: A review of the maximum entropy production principle, Rev. Geophys., 41, 1018, doi:10.1029/2002RG000113, 2003.

Pausch, R. C., Grote, E. E., and Dawson, T. E.: Estimating water use by sugar maple trees: considerations when using heat-pulse methods in trees with deep functional sapwood, Tree Physiol., 20, 217–227, 2000.

Priestley, C. and Taylor, R.: On the assessment of surface heat flux and evaporation using large-scale parameters, Mont. Eeather Rev., 100, 81–92, 1972.

R Core Team: R: A Language and Environment for Statistical Computing, R Foundation for Statistical Computing, Vienna, Austria, http://www.R-project.org/, 2016.

Raupach, M. R.: Combination theory and equilibrium evaporation, Quarterly J. Roy. Meteorol. Soc., 127, 1149–1181, doi:10.1002/qj.49712757402, 2001.

Roberts, J.: Forest transpiration: A conservative hydrological process?, J. Hydrol., 66, 133–141, doi:10.1016/0022-1694(83)90181-6, 1983.

Saveyn, A., Steppe, K., and Lemeur, R.: Spatial variability of xylem sap flow in mature beech (Fagus sylvatica) and its diurnal

dynamics in relation to microclimate, Botany, 86, 1440–1448, doi:10.1139/B08-112, 2008.

Schipka, F., Heimann, J., and Leuschner, C.: Regional variation in canopy transpiration of Central European beech forests, Oecologia, 143, 260–270, doi:10.1007/s00442-004-1798-6, 2005.

Schmidt, M.: Canopy transpiration of beech forests in Northern Bavaria - Structure and function in pure and mixed stands with oak at colline and montane sites, Doctoral thesis, Bayreuth, 2007.

Schmidt, W.: Strahlung und Verdunstung an freien Wasserflächen; ein Beitrag zum Wärmehaushalt des Weltmeers und zum Wasserhaushalt der Erde, Ann. Calender Hydrographie und Maritimen Meteorologie, 43, 111–124, 1915.

Schweingruber, F. H., Bärner, A., and Schulze, E. D.: Atlas of Woody Plant Stems: Evolution, Structure, and Environmental Modifications, Springer Science & Business Media, 2006.

Schwinning, S.: The ecohydrology of roots in rocks, Ecohydrology, 3, 238–245, doi:10.1002/eco.134, 2010.

Schwärzel, K., Menzer, A., Clausnitzer, F., Spank, U., Häntzschel, J., Grünwald, T., Kästner, B., Bernhofer, C., and Feger, K.-H.: Soil water content measurements deliver reliable estimates of water fluxes: A comparative study in a beech and a spruce stand in the Tharandt forest (Saxony, Germany), Agr. For. Meteor., 149, 1994–2006, doi:10.1016/j.agrformet.2009.07.006, 2009.

Shinohara, Y., Tsuruta, K., Ogura, A., Noto, F., Komatsu, H., Otsuki, K., and Maruyama, T.: Azimuthal and radial variations in sap flux density and effects on stand-scale transpiration estimates in a Japanese cedar forest, Tree Physiol., 33, tpt029, doi:10.1093/treephys/tpt029, 2013.

Shuttleworth, W.: Evaporation. Handbook of Hydrology, DR Maidment, Ed, McGraw-Hill, New York, NY, USA, 1993.

Stull, R. B.: An introduction to boundary layer meteorology, vol. 13, Kluwer Academic Publishers, Dordrecht, The Netherlands, 1988.

Šúri, M. and Hofierka, J.: A New GIS-based Solar Radiation Model and Its Application to Photovoltaic Assessments, T. GIS, 8, 175–190, doi:10.1111/j.1467-9671.2004.00174.x, 2004.

Teskey, R. O. and Sheriff, D. W.: Water use by Pinus radiata trees in a plantation, Tree Physiol., 16, 273–279, doi:10.1093/treephys/16.1-2.273, 1996.

Tromp-van Meerveld, H. J. and McDonnell, J. J.: On the interrelations between topography, soil depth, soil moisture, transpiration rates and species distribution at the hillslope scale, Adv. Water Resour., 29, 293–310, doi:10.1016/j.advwatres.2005.02.016, 2006.

Vandegehuchte, M. W. and Steppe, K.: Improving sap flux density measurements by correctly determining thermal diffusivity, differentiating between bound and unbound water, Tree Physiol., 32, 930–942, doi:10.1093/treephys/tps034, 2012a.

Vandegehuchte, M. W. and Steppe, K.: Sapflow+: a four-needle heat-pulse sap flow sensor enabling nonempirical sap flux density and water content measurements, New Phytol., 196, 306–317, doi:10.1111/j.1469-8137.2012.04237.x, 2012b.

Vandegehuchte, M. W. and Steppe, K.: Sap-flux density measurement methods: working principles and applicability, Funct. Plant Biol., 40, 213–223, 2013.

Wang, J. and Bras, R. L.: A model of evapotranspiration based on the theory of maximum entropy production, Water Resour. Res., 47, W03521, doi:10.1029/2010WR009392, 2011.

Wang, Y. and Jarvis, P.: Description and validation of an array model - MAESTRO, Agr. For. Meteorol., 51, 257–280, doi:10.1016/0168-1923(90)90112-J, 1990.

West, G. B., Brown, J. H., and Enquist, B. J.: A general model for the structure and allometry of plant vascular systems, Nature, 400, 664–667, doi:10.1038/23251, 1999.

Whitehead, D.: Regulation of stomatal conductance and transpiration in forest canopies, Tree Physiol., 18, 633–644, doi:10.1093/treephys/18.8-9.633, 1998.

Wilson, K. B., Hanson, P. J., Mulholland, P. J., Baldocchi, D. D., and Wullschleger, S. D.: A comparison of methods for determining forest evapotranspiration and its components: sap-flow, soil water budget, eddy covariance and catchment water balance, Agr. For. Meteorol., 106, 153–168, 2001.

Wullschleger, S. D. and King, A. W.: Radial variation in sap velocity as a function of stem diameter and sapwood thickness in yellow-poplar trees, Tree Physiol., 20, 511–518, doi:10.1093/treephys/20.8.511, 2000.

Zapater, M., Hossann, C., Bréda, N., Bréchet, C., Bonal, D., and Granier, A.: Evidence of hydraulic lift in a young beech and oak mixed forest using 18O soil water labelling, Trees, 25, 885–894, doi:10.1007/s00468-011-0563-9, 2011.

Zehe, E., Ehret, U., Pfister, L., Blume, T., Schräder, B., Westhoff, M., Jackisch, C., Schymanski, S. J., Weiler, M., Schulz, K., Allroggen, N., Tronicke, J., van Schaik, L., Dietrich, P., Scherer, U., Eccard, J., Wulfmeyer, V., and Kleidon, A.: HESS Opinions: From response units to functional units: a thermodynamic reinterpretation of the HRU concept to link spatial organization and functioning of intermediate scale catchments, Hydrol. Earth Syst. Sci., 18, 4635–4655, doi:10.5194/hess-18-4635-2014, 2014.

Zeileis, A.: Econometric computing with HC and HAC covariance matrix estimators, J. Stat. Softw., 11, 1–17, 2004.

Zeileis, A. and Hothorn, T.: Diagnostic checking in regression relationships, R News, 2, 7–10, 2002.

Zhang, L., Potter, N., Hickel, K., Zhang, Y., and Shao, Q.: Water balance modeling over variable time scales based on the Budyko framework – Model development and testing, J. Hydrol., 360, 117–131, doi:10.1016/j.jhydrol.2008.07.021, 2008.

Zhang, Q., Manzoni, S., Katul, G., Porporato, A., and Yang, D.: The hysteretic evapotranspiration-Vapor pressure deficit relation: ET-VPD hysteresis, J. Geophys. Res.-Biogeosci., 119, 125–140, doi:10.1002/2013JG002484, 2014.